THESIS

EVALUATION OF ANALYTICAL FOOTPRINT MODELS AND ENERGY BALANCE CLOSURE METHODS OVER COTTON IN TEXAS PANHANDLE

Submitted by

Stuart L. Joy

Department of Civil and Environmental Engineering

In partial fulfillment of the requirements

For the Degree of Master of Science

Colorado State University

Fort Collins, Colorado

Fall 2011

Master's Committee:

Advisor: José Luis Chávez

Allan A. Andales
Jay Ham

ABSTRACT

EVALUATION OF ANALYTICAL FOOTPRINT MODELS AND ENERGY BALANCE CLOSURE METHODS OVER COTTON IN TEXAS PANHANDLE

Eddy covariance (EC) systems are being used to measure sensible heat (H) and latent heat (LE) fluxes in order to determine crop water use or evapotranspiration (ET). However, EC systems tend to systematically underestimate H and LE fluxes; thus, a lack of energy balance closure. The reliability of EC measurements depends on meeting certain meteorological assumptions; the most important of such are a horizontal homogeneity, stationarity, and non-advective conditions. Over heterogeneous surfaces the spatial context of the measurement must be known in order to properly interpret the magnitude of the heat flux measurement results. Over the past two decades there has been a proliferation of 'heat flux source area' (i.e., footprint) modeling studies but only a few that explore the accuracy of models over heterogeneous agricultural land. A composite ET estimate was created by using the estimated footprint weights for an EC system in the upwind corner of four fields and separate ET estimates from each of these fields. Three analytical footprint models were evaluated by comparing the composite ET to the measured ET. All three models performed consistently with an average MBE of about -0.03 mm h^{-1} (-4.4%) and RMSE of 0.09 mm h^{-1} (10.9%). The same three footprint models were then used to adjust measured ET to account for the fraction of the footprint that extended beyond the field of interest. The effectiveness of the footprint adjustment was determined by comparing adjusted ET estimates with lysimetric ET measurements from within the same field. This correction decreased the absolute hourly ET MBE by 8% and the RMSE by 1%. The energy

balance is rarely closed with the EC method and therefore the energy balance was closed by adjusting the H and LE heat fluxes by first assuming the H was measured accurately and applying the entire residual to the LE (LEC) heat flux and secondly by assuming the Bowen ratio (BRC) was measured accurately and adjusting both H and LE while conserving the BR. The application of energy balance closure to uncorrected EC heat fluxes showed better agreement between EC and lysimeter ET. There was not a significant difference between the BRC and LEC methods when applied to uncorrected heat fluxes.

The analytical footprint models developed by Schuepp et al. (1990), Hsieh et al. (2000), and Kormann and Meixner (2001) all gave a reliable estimate of the footprint for heterogeneous agricultural land under highly advective conditions. Care should be taken when using the EC system to measure ET early in the growth stage of a crop when the surface is smooth because the footprint will extend farther upwind. Correcting the EC heat fluxes for coordinate rotation, density, spectral attenuation, and sonic temperature heat flux and then applying the proposed correction considering the footprint resulted in the most accurate estimate of hourly EC based ET with a MBE of 0.01 mm h^{-1} (0.6 to 1.5%) and RMSE of 0.10 to 0.11 mm h^{-1} (10.6 to 11.66%).

ACKNOWLEDGEMENTS

I would first like to thank my advisor, Dr. José Luis Chávez, for his continued support of my research and the countless hours of instruction and guidance. I also would like to thank my committee members (Drs. Jay Ham and Allan Andales) for their valuable feedback during this process.

I am grateful the Dr. Terry Howell and the staff at the USDA-ARS Conservation Research and Production Laboratory in Bushland, TX for sharing data from the BEAREX08 project. I am also grateful for their comments on my conference and journal papers.

I have fellow graduate students Jordan Varble to thank for his support from day one, Mcebisi Mkhwanazi for his assistance with the remote sensing data processing, Evan Rambikur for the discussions about footprint models and other ET methods, Soheil Kolouri for the help on writing the Matlab code, and Abhinaya Subedi for his exceptional head calculations in the field.

Most of all I am grateful for my loving family that has inspired me to do more than I thought I could accomplish.

For Allyson…

This is a testament of

your love, patience, and support

more than any gain of knowledge or

accomplishment on my part.

TABLE OF CONTENTS

ABSTRACT ii
ACKNOWLEDGEMENTS iv
TABLE OF CONTENTS vi
LIST OF TABLES viii
LIST OF FIGURES ix
CHAPTER 1: INTRODUCTION 1
Measuring Evapotranspiration 1
Energy Balance Closure 3
Flux Footprint Modeling 4
Motivation and Objectives 5
CHAPTER 2: FOOTPRINT VALIDATION AND CORRECTION OF EC ET CONSIDERING HEAT FLUX SOURCE AREA 7
Background 7
Site Description 7
Large Monolith Weighing Lysimeters 8
Eddy Covariance Energy Balance System 9
Eddy Covariance Data Processing 11
Footprint Modeling Methodology 15
Schuepp Model 15
Hsieh Model 16
Crosswind Function 17
Kormann & Meixner Model 18
Footprint Contribution from Each Field 20
Footprint Validation Procedure 20
ET Correction Using Footprint Fractions 21
Statistical Analysis 22
Results and Discussion 22
Surface Roughness 24
Instrument Variability 28
Footprint Validation 28
ET Correction Using Footprint Fractions Evaluation 33

Conclusion 35
CHAPTER 3: EDDY COVARIANCE HEAT FLUX ENERGY BALANCE CLOSURE 37
Background 37
Site Description 37
Large Monolith Weighing Lysimeters 38
Eddy Covariance Energy Balance System 39
Eddy Covariance Data Processing 41
Bowen Ratio Closure 45
Results and Discussion 46
Conclusion 48
CHAPTER 4: CONCLUSION 50
APPENDIX A: EDIRE PROCESSING LIST FOR EC8 58
APPENDIX B: MATLAB CODE FOR S90 AND H2000 FOOTPRINT MODELS 78
APPENDIX C: MATLAB CODE FOR KM01 FOOTPRINT MODEL 80
APPENDIX D: DAILY ET 82

LIST OF TABLES

2.1: Instrumentation details for eddy covariance systems and lysimeter. 11

2.2: Post-processing procedure using the software package EdiRe. 13

2.3: Footprint model inputs and their respective measurement methods. 20

2.4: Comparison of composite ET to ET from EC8. 28

2.5: Comparison of composite ET calculated using combination of lysimeter and EC data to ET from EC8 for different growth stages and the entire study period. 29

2.6: Average Kormann and Meixner cumulative footprint (%) for each field during different growth stages and the entire study period. 30

2.7: Comparison of composite ET calculated using combination of lysimeter and EC data to ET from EC8 for different atmospheric stability regimes. 32

2.8: Comparison of footprint corrected ET from EC8 to Lysimeter (NE) ET for different growth stages and the entire study period. 34

3.1: Instrumentation details for eddy covariance systems and lysimeter. 41

3.2: Post-processing procedure using the software package EdiRe. 43

3.3: Evaluation of latent heat flux and Bowen ratio energy balance closure with and without common corrections for coordinate rotation, density, spectral attenuation, and heat flux correction by comparing EC8 ET to NE lysimeter ET with significant errors in bold face type. 47

3.4: Evaluation of latent heat flux and Bowen ratio energy balance closure with and without common corrections for coordinate rotation, density, spectral attenuation, and heat flux correction by comparing EC9 ET to SE lysimeter ET with significant errors in bold face type. 48

D.1: Daily ET from NE and SE lysimeters, grass reference ET, and precipitation for each DOY during the study period. 83

LIST OF FIGURES

2.1: Lysimeter box with micrometeorological instrumentation (a) and eddy covariance system (b). Photographs courtesy of José Luis Chávez. 9

2.2: Experimental setup at the USDA-ARS, Conservation and Production Research Laboratory, Bushland, TX with the positions of the eddy covariance systems (EC), large weighing lysimeters, and large aperture scintillometers (LAS) and their respective paths (dotted lines) shown. The orientation of the lines corresponds to the orientation of the rows. 10

2.3: Percent data missing and excluded due to quality control parameters..... 15

2.4: Average daily values of the meteorological conditions during the study period. (a) Grass reference ET, (b) air and soil temperature (45 cm), (c) relative humidity [RH] and daily cumulative precipitation, and (d) daily growing degree days [GDD], and cumulative GDD for the East and West fields..... 23

2.5: Wind rose plot (a) and wind class frequency distribution (b) for June 6 – October 10, 2008 using wind data from EC8. 24

2.6: Crop height with respect to time (DOY) for the NE, SE, SW, and NW fields..... 25

2.7: NDVI images with lysimeter fields (solid lines) and weather station grass field (dotted lines) boundaries shown for DOYs 155, 171, 187, 203, 219, and 235 derived from reflectance images courtesy of the U.S. Geological Survey..... 27

2.8: Mean NDVI with standard deviation (bars) for (a) NW, (b) NE, (c) SW, and (d) SE fields on DOYs 155, 171, 187, 203, 219, and 235..... 27

2.9: The change in the ratio u/u_* over time as the crop canopy develops for NE field..... 31

2.10: Contour plots of footprints at EC1 using S90 (a), H2000 (b), and KM01 (c) models during stable stratification on DOY 218 at 6:30 am CST. 32

2.11: One dimensional plot of footprints at EC1 using S90 (a), H2000 (b), and KM01 (c) models during stable stratification on DOY 218 at 6:30 am CST..... 33

2.12: Contour plots of footprints at EC1 using S90 (a), H2000 (b), and KM01 (c) models during unstable stratification on DOY 195 at 14:30 am CST. 33

2.13: One dimensional plot of footprints at EC1 using S90 (a), H2000 (b), and KM01 (c) models during unstable stratification on DOY 195 at 14:30 am CST..... 33

3.1: Lysimeter box with micrometeorological instrumentation (a) and eddy covariance system (b). Photographs courtesy of José Luis Chávez. 39

3.2: Experimental setup at the USDA-ARS, Conservation and Production Research Laboratory, Bushland, TX with the positions of the eddy covariance systems (EC), large weighing lysimeters, and large aperture scintillometers (LAS) and their respective paths (dotted lines) shown. The orientation of the lines corresponds to the orientation of the rows. 40

CHAPTER 1: INTRODUCTION

The trends of river depletion and groundwater overdraft in arid and semi arid regions of the world have sparked extensive discussion on how to meet the water demands of a growing population. In the U.S., irrigation accounts for 37% of total freshwater withdrawals (62% for all categories excluding thermoelectric power) of which 85% is in the 17 conterminous arid western states (Kenny et al. 2009). Worldwide, irrigation accounts for about 80% of the total freshwater consumed and is responsible for more than 40% of all agricultural production (Hoffman et al. 2007). Irrigated agriculture is not only needed to meet the food demand of a growing population but also to alleviate world hunger by meeting the United Nations Millennium Development Goals. This dilemma is further exacerbated by the concern of global climate change. The efficient use of irrigation water is largely dependent on understanding the plant consumptive water use through the process of evapotranspiration (ET).

Measuring Evapotranspiration

Measuring and modeling ET is difficult due to the nature of water vapor transport into the atmosphere. Allen et al. (2011) discussed factors governing measurement accuracy for the following methods:

1. Soil water balance
2. Lysimetry
3. Energy Balance Bowen Ratio (EBBR)
4. Eddy Covariance (EC)
5. Scintillometry
6. Sap Flow
7. Remote Sensing and Satellite-based Modeling

Soil water balance is an affordable and relatively accurate method that can be used for irrigation scheduling. However, for a novice or a person working outside their specialty, errors in measurement can be 20-70% (Allen et al. 2011). Methods 2-7 require expensive instrumentation and expert operators. Remote sensing and satellite-based modeling holds great potential for practical application since the process covers large areas that can be instantaneously available via the internet. Sap flow methods directly measure the transpiration through a plant but large errors are introduced when attempting to scale up measurements to a field or regional scale. Methods 2-5 are primarily used in research and are being used to calibrate and validate remote sensing models. Properly managed lysimeters have the potential of measuring ET with high accuracy, according to Howell et al. (1995). However, these instruments are large, expensive, and only provide the user with a point measurement in space. Methods 3 and 5 are micrometeorological approaches that are based on the conservation of energy. The major components of the energy balance are net radiation (R_n), soil heat flux (G), sensible heat flux (H), and latent heat flux (LE) all in units of W m^{-2} and can be expressed as:

$$R_n - G = H + LE \tag{1.1}$$

where the left side in Eq. (1.1) is defined as available energy (R_n-G) and the right side as turbulent fluxes (H+LE) with the signal convention of positive away from the surface with the exception of R_n. The EBBR method uses measurements of R_n, G, and gradients of temperature and water vapor in the atmosphere to estimate the ratio H/LE. The EC method is based on the direct measurement of high frequency vertical wind (w) and a scalar concentration (c), such as water vapor or air temperature, producing LE [Eq. (1.2)] and H [Eq. (1.3)], respectively, assuming the mean vertical velocity is negligible:

$$LE = \rho_a \lambda \overline{w'q'} \tag{1.2}$$

$$H = C_p \rho_a \overline{w'T'} \tag{1.3}$$

where q is the air specific humidity (kg kg^{-1}), T is the air temperature (°C), ρ_a is the moist air density (kg m^{-3}), C_p is the specific heat of dry air at constant pressure (J kg^{-1} K^{-1}), λ is the latent heat of water vaporization (J kg^{-1}), which varies with air temperature (T, °C), and the primes denote the deviation or fluctuation from the mean (e.g., $x' = x - \overline{x}$). Since EC takes measurements above the transpiring canopy, the temperature and scalar concentrations sampled are actually a mixture of downwind point sources. The EC system has the advantage that it can be easily relocated, and that its derived *H* and *LE* values are representative of its given source area.

Energy Balance Closure

It has been well documented in the literature that eddy covariance systematically tends to underestimate surface scalar fluxes and thus fails to close the energy balance (Mahrt 1998; Aubinet et al. 1999; Oncley et al. 2007; Wilson et al. 2002). Energy balance closure is expressed as a percentage and typically ranges from 70-80% (i.e., a 20-30% lack of closure).

$$Energy\ Balance, \% = \left(\frac{H + LE}{R_n - G} \right) * 100 \qquad (1.4)$$

Foken (2008) provides an overview of the energy balance closure problem and states that the problem can no longer be attributed to storage terms in the upper soil layer and measurement error, but suggests that it is a scale problem in which larger eddies that cannot be measured by EC are generated at boundaries between different land uses. These larger eddies are absent over homogeneous surfaces as shown in the experiment NIMEX-1 in Il-Ife, Nigeria (Mauder et al. 2007) where the energy balance closure over a homogeneous fallow bush-land was 95%.

Turbulent motions of periods longer than the averaging period cannot contribute to the eddy flux. By extending the averaging period, low frequency turbulence is captured and the flux increases. However, too long of an averaging period may include unwanted non-stationary signals and thus introduce more error (Lee et al. 2004).

Flux Footprint Modeling

The 'heat flux source area' (i.e., footprint) is the portion of the upwind surface of the EC instrumentation site containing the effective heat flux sources/sinks contributing to a flux or concentration observation at a certain measurement height (Schmid and Oke 1990; Schuepp et al. 1990). If the EC system is located within the constant flux layer over an extended homogeneous surface then the position of the sensor is not an issue. However, over a heterogeneous surface (e.g., patchwork of agricultural land) the location and size of the flux footprint is needed to interpret the measured flux (i.e., to understand the source area of the heat fluxes). As a result there has been a proliferation of footprint modeling research since 1990. There are four theoretical approaches: analytical models, Lagrangian-stochastic particle dispersion models, large-eddy simulations, and ensemble-averaged closure models. Extensive reviews of these approaches are presented by Schmid (2002) and Vesala et al. (2008). The latter three approaches are mathematically complicated and thus resource intensive. Analytical models can be misleading if used in conditions that violate the underlying assumptions of each particular model (Schmid 2002; Vesala et al. 2008). Nevertheless, analytical models can easily be applied to processing code and thus be used to filter and correct flux measurements quickly in post-processing or possibly in real time if programmed in the datalogger. The analytical footprint models of Hsieh et al. (2000) and Kormann and Meixner (2001) have been used as quality control filters for EC data collected over various land covers (Ortega-Farias et al. 2004; Saito et al. 2005; Rogiers et al. 2005; Hammerle et al. 2007) and used to scale and validate remotely sensed energy balance models (Li et al. 2008; Timmermans et al. 2008; Chen et al. 2009). The Kormann and Meixner model (2001) is also employed by the frequently used open source EC data processing software EdiRe (Clement 1999) and TK3 (Mauder and Foken 2011). Inter comparison of footprint models has been the primary method of validating footprint models in the past (Leclerc and Thurtell 1990; Hsieh et al. 2000; Kljun et al. 2003). Foken and Leclerc (2004) proposed three methods for 'in situ' validation of models: (1) the use of artificial tracers, (2) the use of

natural tracers, and (3) the effect of isolated heterogeneities. If a suitable artificial tracer is chosen there is the advantage of there not being any other source or sink for the tracer. The disadvantages to artificial tracers are the difficulty of approximating natural field conditions and the expense of setting up these experiments. Natural tracer validation methods are both inexpensive and easier to use. Cooper (2003) used water vapor as a natural tracer and found good agreement between point flux measurements of ET, lidar-derived moisture fluxes, and a footprint model. By comparing measurements from two adjoining surfaces and that of the two surfaces combined Beyrich et al. (2002) found that Lagrangian stochastic simulation (Rannik et al. 2000) better represented the flux contribution from different fields than Schmid's analytical model (1997). Marcolla and Cescatti (2005) compared three analytical models by comparing measurements from an alpine meadow before and after cutting to those during an intermittent time when only a portion of the meadow was cut. As a result they found that the Schuepp (1990) model generally overestimates the footprint and that all models do not perform well in very unstable conditions.

Motivation and Objectives

Analytical footprint models have been extensively studied for different atmospheric conditions and compared to other more sophisticated models (e.g. Lagrangian stochastic). Only a few studies have explored the accuracy of such models over irrigated cropland surrounded by rainfed crops and/or fallow land. Also, there has not been a study that has explored correcting flux measurements for a footprint that extends beyond the area of interest. Therefore the first objective of this study is to compare the performance of the Scheupp et al. (1990), Hsieh et al. (2000) and Kormann and Meixner (2001) analytical footprint models over irrigated cotton adjacent to dryland cotton and evaluate a method for improving the LE flux, measured by an EC system, by accounting for the footprint fraction that extends beyond the irrigated field boundaries.

The energy balance closure problem continues to be an ongoing issue with the EC method. This issue is being aggressively studied by researchers in the micrometeorology,

engineering, and environmental fields of study. Inevitably, more physically based solutions will be developed but in the meantime researchers in the remote sensing field of study need reliable flux estimates from EC to validate models. Twine et al. showed that only a 6-7% bias in the energy balance can be attributed to the available energy and therefore the deficit in the energy balance is most reasonably removed by adjusting H and LE (Twine et al. 2000; Chávez et al. 2009). That study also presented two options for closing the energy balance: 1. Assume H is accurately measured and solve for LE as a residual to the energy balance equation or 2. Assume that the Bowen ratio (BR) is correctly measured by the EC system and adjust both H and LE while conserving the BR. What previous research has not explored is the effect of closing the energy balance after applying a common suite of corrections to the EC-based fluxes found in the literature and how well these closure methods work under a highly advective environment. Thus the second objective of this study is to evaluate the application of these two methods of energy balance closure before and after applying common corrections.

CHAPTER 2: FOOTPRINT VALIDATION AND CORRECTION OF EC ET CONSIDERING HEAT FLUX SOURCE AREA

Background

The Bushland Evapotranspiration and Agricultural Remote Sensing Experiment 2008 (BEAREX08) was conducted during the 2008 cotton cropping season at the USDA-ARS Conservation and Production Research Laboratory (CPRL), located at Bushland, TX. Researchers from eight federal and state institutions evaluated the ability of land surface energy balance and crop coefficient-based ET models to estimate ET at point, plot, field, and regional scales in a semi-arid, highly advective agricultural region. Instrumentation for the project included aircraft flux and remote sensing, a tethered sonde system, a network of soil moisture, heat flux, and temperature sensors, three Bowen Ratio stations, three large aperture scintillometers, nine EC stations, and four large precision weighing lysimeters (Evett et al. 2011a, 2009).

Site Description

For this study the data from BEAREX08 was used. The geographic coordinates of the CPRL are 35°11'N, 102°06'W, and its elevation is 1,170 m above mean sea level. Soils in and around Bushland are classified as slowly permeable Pullman clay loam. The major crops in the region are corn, sorghum, winter wheat, and cotton. Wind direction is predominantly from the south/southwest direction. The average precipitation that occurs during the cotton growing season (May-October) is 350 mm (Howell et al. 2004). About 600 mm of irrigation, precipitation, and soil water are needed to grow cotton (New 2008), thus irrigation needs to provide about 250 mm of timely water for a successful cotton harvest. The typical growing season grass reference ET is 6.0-8.2 mm day^{-1} (Howell et al. 2004). In addition, the long-term

annual microclimatological conditions indicate that the study area is subject to very dry air and strong winds. Growing season averages at Bushland for air temperature and horizontal wind speed are 20°C and 3.9 m s^{-1}, respectively (Howell et al. 2004).

Large Monolith Weighing Lysimeters

Precision weighing lysimeters (Marek et al. 1988), $3 \times 3 \times 2.3$–m deep, were used to measure cotton ET. Each lysimeter contained a monolithic Pullman clay loam soil core. The lysimeters were located at the center of four fields (210 m East-West by 225 m North-South) two (East) irrigated by a linear move system and two (West) not irrigated. The change in lysimeter mass was measured by load cell (SM-50, Interface, Scottsdale, Ariz.) and recorded by a datalogger (CR7-X, Campbell Scientific Inc., Logan, Utah). The signal was sampled at 0.17 Hz frequency. The high frequency load cell signal was averaged for 5 min and composited to 15-min means. The lysimeter was calibrated as explained in Howell et al. (1995). The lysimeter mass measurement accuracy in water depth equivalent was 0.01 mm, as indicated by the RMSE of calibration. A simple soil water balance using change in water storage from four neutron probes, irrigation, and precipitation data showed that the Northeast (NE) lysimeter had a larger ET than the surrounding field (Evett et al. 2011b). According to that study, the ET measurements from the NE lysimeter were 18% larger than the surrounding field from DOY 182 to 220 due to greater leaf area index (LAI) on the lysimeter than the surrounding field. Therefore, the NE lysimeter ET measurements, from that period, were reduced by 18% in order to ensure they were representative of the entire field. Pictures of a lysimeter box and an EC system are shown in Figure 2.1.

Figure 2.1: Lysimeter box with micrometeorological instrumentation (a) and eddy covariance system (b). Photographs courtesy of José Luis Chávez.

Eddy Covariance Energy Balance System

Five EC systems (EC1, EC2, EC3, EC5, and EC8) out of the nine from BEAREX08 experiment were used to monitor the exchange of heat fluxes at different parts of the CPRL site. The instrument positions are shown in Figure 2.2. Instrumentation details of all systems used are given in Table 2.1. Time series data consisted of horizontal (u), lateral (v), and vertical (w) wind vectors (m s^{-1}), calculated sonic temperature (T_s, ºC), water vapor concentration (H_2O, g m^{-3}), carbon dioxide concentration (CO_2, mg m^{-3}), and atmospheric pressure (P, kPa), all measured at a frequency of 20 Hz. The CSAT3 sensor was oriented toward the predominant wind direction, with an azimuth angle of 225° from true North for EC8 and 180° for systems EC1, EC2, EC3, and EC5. Installed within and between the crop rows, about 4 m east from each EC system, were instruments for measuring soil heat flux, soil temperature, and soil volumetric water content. The temperature and water content data were used to calculate soil heat storage in the layer between the surface and the depth of soil heat flux plate installation. Soil heat flux plates (SHFP) were installed at 0.08 m depth within and between crop rows. Soil thermocouple pairs were installed at 0.02 and 0.07 m depths close to the SHFP locations. Soil water content reflectometers (CS616, Campbell Scientific Inc., Logan, UT) were installed slanted at an approximate angle of 13

degrees across the 0.01-0.1 m depth to measure the volumetric soil water content in this depth zone. Water content reflectometers were field cross-calibrated against water contents reported by a conventional time domain reflectometry (TDR) (TR-100, Dynamax, Inc., Houston, TX) system that used a soil-specific calibration that minimized soil temperature influences on the TDR water contents readings (Evett et al. 2005). Soil temperature was sensed and recorded during the cross-calibration and a soil temperature correction was developed for the CS616 data (Evett and Schwartz 2009).

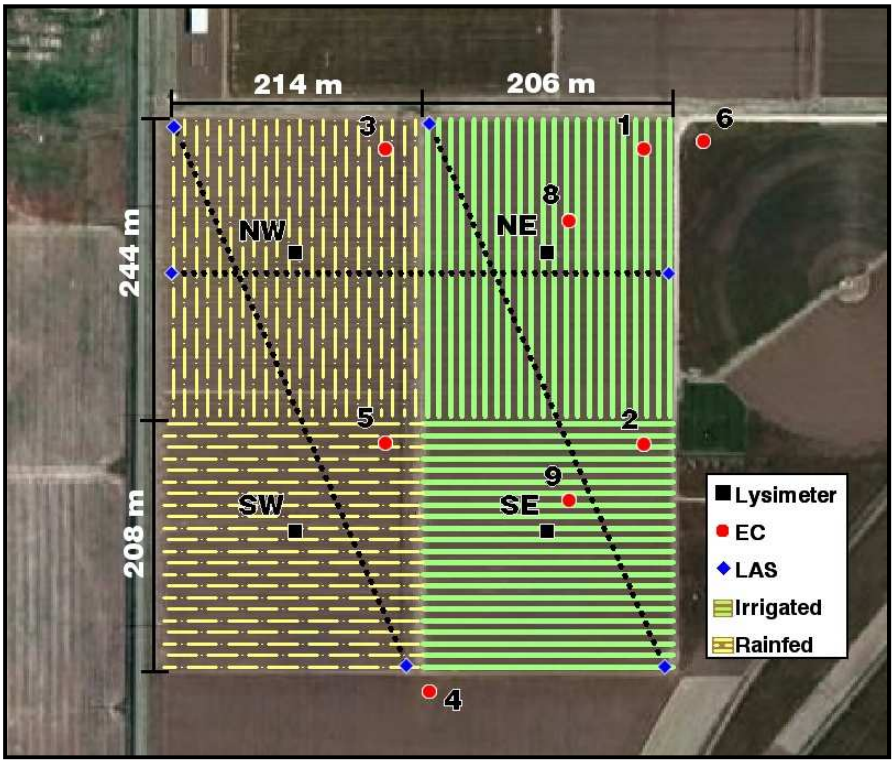

Figure 2.2: Experimental setup at the USDA-ARS, Conservation and Production Research Laboratory, Bushland, TX with the positions of the eddy covariance systems (EC), large weighing lysimeters, and large aperture scintillometers (LAS) and their respective paths (dotted lines) shown. The orientation of the lines corresponds to the orientation of the rows.

Table 2.1: Instrumentation details for eddy covariance systems and lysimeter.

Instrument	EC8	EC1, EC2, EC3, EC5	Lysimeters
3D Sonic Anemometer	CSAT3[a]	CSAT3[a]	—
Open Path Gas Analyzer	LI-7500[b]	LI-7500[b]	—
Fine Wire Thermocouple	FW05[a]	FW05[a]	—
Air Temp/ Relative Humidity	HMP45C[c]	HMP45C[c]	HMP45C[c]
Barometer	CS106[a]	—	—
Net Radiometer	—	CNR1[e]	REBS Q*7.1[d], K&Z CM14[e], K&Z CGR3[e]
Soil Heat Flux Plates	(2) REBS HFT-3[d]	(3) REBS HFT-1.1[d]	(4) REBS HFT-1.1[d]
Soil Temperature	(4) TCAV[a]	(6) TMTSS-020G-6[f]	(8) TMTSS-020G-6[f]
Soil Water Content	(2) CS616[a]	(3) CS616[a]	—
Precipitation Gauge	—	—	Qualimetrics 6011B[g]
Datalogger	CR3000[a]	CR5000[a]	CR7X[a]
CSAT Azimuth	225°	180°	—
Measurement Height	2.5 m	2.25 m	—
Sampling frequency	20 Hz[g]	20 Hz[g]	0.17 Hz

Eddy Covariance Data Processing

Time series, high frequency, EC data were post-processed with the EdiRe software package (Clement 1999) following the guidelines described in Lee et al. (2004) and Burba and Anderson (2010) as summarized in Table 2.2 (detailed EdiRe processing file shown in Appendix A). EdiRe is a fast and flexible software tool that allows rapid redesign of routines to enhance question/answer cycle of data analysis. Before covariances were calculated, spikes of six standard deviations from the population mean were removed from the time series. If four or more consecutive data points were detected with values larger than standard deviation then they were not considered as a spike (Vickers and Mahrt 1997). Time delay between the CSAT3 and LI-7500 was removed using a cross-correlation analysis (McMillen 1988). Although the terrain for the site was practically flat, the CSAT3 cannot be perfectly leveled, such that the vertical component (w) is perpendicular to the mean streamline plane. For this reason, the coordinates were rotated using the double rotation method (Kaimal and Finnigan 1994). According to Lee et

al. (2004) this method is suitable for ideal sites with little slope and fair weather conditions. The effects of density fluctuations induced by heat fluxes on the measurement of eddy fluxes of water vapor using the LI-7500 were corrected using the procedure outlined by Webb et al. (1980). Spectral loss in the high frequency band due to path-length averaging, sensor separation, and signal processing was corrected after Moore (1986). Data from the fine wire thermocouple was intermittent due to equipment failure and thus sonic temperature (T_s) was used in sensible heat flux calculation. Schotanus et al. (1983) recommended correcting T_s for crosswind and humidity effects, commonly referred to as the heat flux correction. The CSAT3 implements the crosswind correction online and therefore the heat flux only needed to be corrected for humidity fluctuations. The sonic temperature flux $\overline{w'T_s'}$ was converted to actual temperature flux $\overline{w'T'}$ following the method of Schotanus et al. (1983).

A dimensionless parameter that characterizes the processes in the surface layer is the atmospheric stability parameter (ζ), Eq. (2.2), which is the ratio of the convective production to the mechanical production of turbulent kinetic energy (Campbell and Norman 1998):

$$\zeta = -\frac{0.4 z_m g H}{(T + 273.15)\rho_a C_p u_*^3} \tag{2.1}$$

where, z_m is the horizontal wind speed observation height above the zero-plane displacement height (i.e., z_m=z-d), g is the gravitational acceleration (9.8 m s^{-2}), u_* is the friction velocity (m s^{-1}) and H, T, ρ_a, and C_p are as defined above. Positive ζ represents a stable stratification, negative ζ represents an unstable stratification, and $|\zeta|$<0.02 represents a neutral stratification.

Table 2.2: Post-processing procedure using the software package EdiRe.

Procedure		EdiRe Commands
1	Extract raw time series data	Extract
2	Calculate wind direction	Wind direction
3	Remove spikes	Despike
4	Calculate and remove lag between instruments	Cross correlate, Remove lag
5	Rotate coordinates	Rotation coefficients, Rotation
6	Calculate means, standard deviations, skewness, and kurtosis	1 chn statistics
7	Calculate covariances and fluxes	Latent heat of evaporation, Sensible heat flux coefficient, 2 chn statistics
8	Calculate friction velocity and stability	User defined, Stability - Monin Obukhov
9	Calculate and apply frequency response corrections	Frequency response
10	Calculate and apply Schotanus H correction	Sonic T - heat flux correction
11	Calculate and apply WPL correction	Webb correction
12	Iterate steps 8-11 two times	
13	Convert LE to ET (mm h^{-1})	User defined
14	Calculate roughness length	Roughness length (z_0)
15	Calculate stationarity	Stationarity

The canopy heights (h_c, m) and leaf area index (LAI, m^2 m^{-2}) for the NE and Southeast (SE) fields were measured five times during the study on the following days of the year (DOY): 171, 182, 200, 210, and 220. Field measurements were taken for the Northwest (NW) and Southwest (SW) fields three times on DOYs 200, 210, and 220. Crop emergence for the East and West fields occurred on DOY 150 and 165, respectively. Curves were fitted to h_c vs. DOY and LAI vs. DOY data to determine the h_c and LAI as functions of the DOY. The analytical expression from Raupach (1992, 1994; 1995) was used to estimate the zero-plane displacement height (d, m).

$$d = h_c - h_c\left[\frac{1-\exp\left(-\sqrt{c_{d1}\Lambda}\right)}{\sqrt{c_{d1}\Lambda}}\right] \tag{2.2}$$

where, c_{d1} is an empirical constant estimated from laboratory and field data to be on the order of 7.5 (Raupach 1994) and Λ is the canopy area index which for unstressed, growing canopies is equivalent to LAI.

Quality control criteria were set for wind direction, stationarity, and integral turbulence characteristics. The percent of data missing and excluded due to each quality control parameter and all parameters combined for each EC system is shown in Figure 2.3. Flow from behind the sensor can be distorted by the instrumentation. Therefore, any data with a wind direction beyond ±90° of the orientation of the sonic anemometer were excluded from further analysis.

Estimates of fluxes via the eddy covariance method are based on simplified forms of the Navier-Stokes equations for certain atmospheric conditions (Stull 1988). These conditions are not always met and therefore must be evaluated. Tests for stationarity and integral turbulence were performed following methods outlined in Foken and Wichura (1996) and Thomas and Foken (2002). For the stationarity test, covariances between the vertical wind speed (w) and the horizontal wind speed (u) and the air temperature (T) and water vapor (q) scalars for the averaging period of 60-min were compared to covariances of consecutive 5-min intervals within the same period. The periods where deviations, Δ_{st}, were greater than 30% were considered unstationary and excluded from the study:

$$\Delta_{st} = \frac{100\left|\overline{w'x'_5} - \overline{w'x'_{60}}\right|}{\overline{w'x'_{60}}} \tag{2.3}$$

where, x is u for momentum flux and the scalar of interest (T or q) for scalar fluxes and *5* and *60* are subscripts for the 5-min and 60-min covariances, respectively. Integral turbulence tests are used to determine if the turbulence is well developed. With weak turbulence the measuring methods based on surface layer similarities may not be valid (Foken et al. 2004). The integral turbulence test was done by comparing measured similarity functions ($\varphi_{measured}$) for vertical wind speed (φ_w) and temperature (φ_T) with modeled functions (φ_{model}) shown in Table 1 of Thomas and Foken (2002).

$$\varphi_w = \frac{\sigma_w}{u_*} \tag{2.4}$$

$$\varphi_T = \frac{\sigma_T}{T_*} \tag{2.5}$$

where, σ_w and σ_T are the standard deviations of w and T, respectively, and T_* is the dynamic temperature (°C). Any periods with deviations between measured and modeled similarity functions, Δ_{ITT}, greater than 30% were excluded:

$$\Delta_{ITT} = \frac{100\left|\varphi_{\mathrm{mod}\,el} - \varphi_{measured}\right|}{\varphi_{\mathrm{mod}\,el}} \tag{2.6}$$

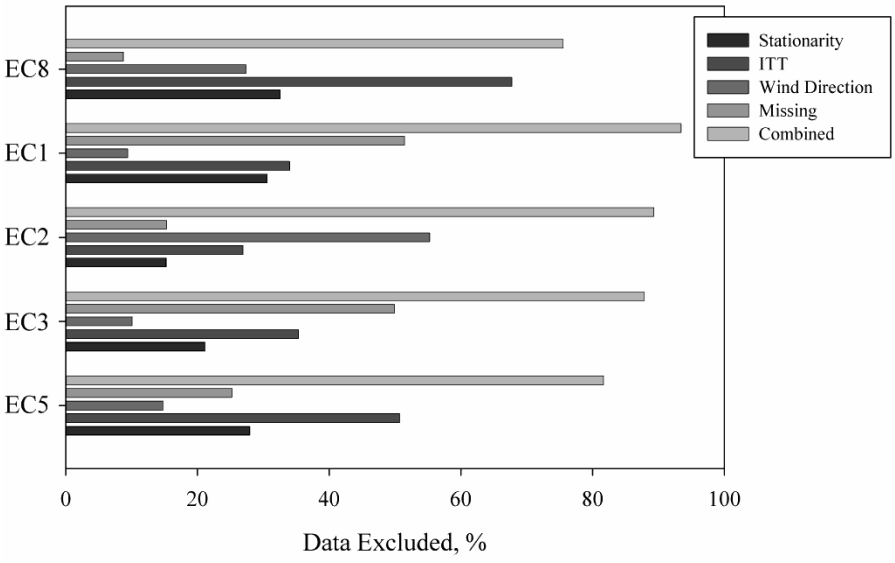

Figure 2.3: Percent data missing and excluded due to quality control parameters.

Footprint Modeling Methodology

The analytical footprint models proposed by Schuepp et al. (1990), Hsieh et al. (2000), and Kormann and Meixner (2001) were used to determine the flux footprint weight per unit source area (i.e., 1-m x 1-m), hereafter referred to as S90, H2000, and KM01, respectively.

Schuepp Model

The S90 model views the transpiring vegetative surface as a continuum of upwind line sources, each occupying an infinitesimal strip of width δx. As proposed by Gash (1986), the approximate analytical solution by Calder (1952) was applied to the basic advection-diffusion

equation, assuming neutral stability and uniform wind velocity. After differentiating with respect to z_m and then integrating with respect to upwind distance (x), an equation for vertical concentration gradient at z_m is reached.

$$\frac{\partial \rho_v(z_m)}{\partial z_m} = -\frac{Q_0}{k u_* z_m} \exp\left(-\frac{U z_m}{k u_* x}\right) \tag{2.7}$$

where, k is von Kármán's constant (0.41), Q_0 is the area flux density, and U is the uniform wind velocity (m s^{-1}) which is defined as the average wind velocity between the surface and z_m (m), assuming a logarithmic profile for $u(z)$.

$$U = \frac{u_*\left[\ln\left(z_m/z_0\right) - 1 + z_0/z_m\right]}{k\left(1 - z_0/z_m\right)} \tag{2.8}$$

where, z_0 is the surface roughness length (m). The relative contribution to the vertical flux at height z_m, $f(x,z_m)$, is then obtained by taking the derivative of Equation (2.7) and multiplying by ku_*z_m.

$$f\left(x, z_m\right) = \frac{k u_* z_m \left(d\rho/dz\right)}{Q_0} = \frac{U z_m \varphi_M}{k u_* x^2} \exp\left(-\frac{U z_m \varphi_M}{k u_* x}\right) \tag{2.9}$$

where φ_M is the momentum correction for stability which is a function of Monin-Obukhov stability parameter ζ (Dyer 1974).

$$\varphi_M = \begin{cases} \left(1 - 16\zeta\right)^{-1/4} & for \zeta < 0 \\ 1 + 5\zeta & for \zeta > 0 \end{cases} \tag{2.10}$$

Hsieh Model

The H2000 model is a hybrid approach which fits Calder's analytical solution (1952) to the results of the numerical Lagrangian model of Thompson (1987). In the analysis of their results, Hsieh et al. (2000) scaled Gash's (1986) effective fetch with the Monin-Obukhov stability length (L, m), and accounted for the effects of stability by introducing the similarity parameters D and P, so that:

$$\frac{x}{|L|} = -\frac{D\left(z_u / |L|\right)^P}{k^2 \ln(F)} \tag{2.11}$$

with

$$z_u = z_m\left[\ln\left(z_m / z_0\right) - 1 + z_0 / z_m\right] \tag{2.12}$$

where *D* and *P* are found by regression of Equation (2.11) to the Lagrangian model results for unstable (*D=0.28, P=0.59*), near-neutral (*D=0.97, P=1*), and stable stratification (*D=2.44, P=1.33*). Rearranging Equation (2.11) and differentiating with respect to x results in the analytical footprint expression:

$$f\left(x, z_m\right) = \frac{D {z_u}^P |L|^{(1-P)}}{k^2 x^2} \exp\left(-\frac{D {z_u}^P |L|^{(1-P)}}{k^2 x}\right) \tag{2.13}$$

Crosswind Function

Both S90 and H2000 are one-dimensional (1-D) footprint models [i.e., expressed along the mean wind direction (*x*)]. The KM01 model is a two-dimensional (2-D) model that expresses the footprint in the mean wind direction and the crosswind direction (*y*). The S90 and H2000 models were expanded into 2-D models so results could be compared to KM01. Diffusion in the lateral direction is commonly assumed to have a Gaussian distribution centered on the mean wind direction:

$$D_y(x, y) = \frac{1}{\sqrt{2\pi}\sigma_y} \exp\left(-\frac{y^2}{2{\sigma_y}^2}\right) \tag{2.14}$$

where D_y is the crosswind concentration distribution function, σ_y is the standard deviation of the lateral spread of the source area and can be related to the plume travel time, $x/\bar{u}_p$, and the standard deviation of lateral wind fluctuations, σ_v as $\sigma_y \approx \sigma_v \cdot x/\bar{u}_p$ (Pasquill 1974; Schmid 1994; Kormann and Meixner 2001; Chen et al. 2009). The Gaussian distribution was combined with H2000 and S90 to expand them into 2-D footprint models:

$$f(x,y,z_m) = f(x,z_m)D_y(x,y) \tag{2.15}$$

Kormann & Meixner Model

The KM01 model uses the solution of the resulting two-dimensional advection-diffusion equation for power law profiles of the mean wind velocity and the eddy diffusivity. The mathematical framework is a stationary gradient diffusion formulation with height-independent crosswind dispersion. The profile parameters are determined by equating the power law to Monin-Obukhov similarity profiles. The complete mathematical description is given by Kormann and Meixner (2001). However, a condensed set of formulas similar to that presented by Neftel et al. (2008) is presented here. First, the profiles of horizontal wind speed and the vertical eddy diffusivity are described by power law relationships:

$$u(z) = \alpha_u z^m \tag{2.16}$$

$$K(z) = \alpha_\kappa z^n \tag{2.17}$$

The proportionality constants α_u and α_κ and the exponents m and n are determined by comparing Eq. (2.16) and (2.17) to the respective Monin-Obukhov similarity profiles at height z_m:

$$m = \frac{u_* \varphi_M}{ku} \tag{2.18}$$

$$n = \frac{z_m}{K}\frac{dK}{dz_m} = \begin{cases} \dfrac{1}{1+5\varsigma} & for\ \varsigma < 0 \\ \dfrac{1-24\varsigma}{1-16\varsigma} & for\ \varsigma > 0 \end{cases} \tag{2.19}$$

$$\alpha_u = \frac{u_* \varphi_M}{km(z_m)^m} \tag{2.20}$$

$$\alpha_\kappa = \frac{ku_* z_M}{\varphi_H (z_m)^n} \tag{2.21}$$

where φ_H is the dimensionless gradient function of heat profile defined by Dyer (1974) as:

$$\varphi_H = \begin{cases} (1-16\varsigma)^{-1/2} & for \varsigma < 0 \\ 1+5\varsigma & for \varsigma > 0 \end{cases} \tag{2.22}$$

Based on these quantities the shape factor *r* and the constant μ of Equations (2.23) and (2.24) are defined as:

$$r = 2 + m - n \tag{2.23}$$

$$\mu = \frac{1+m}{r} \tag{2.24}$$

Finally, the parameters *A*-*E* shown below are related to the above quantities:

$$A = 1 + \mu \tag{2.25}$$

$$B = \frac{\alpha_u (z_m)^r}{r^2 \alpha_\kappa} \tag{2.26}$$

$$C = \frac{B^\mu}{\Gamma(\mu)} \tag{2.27}$$

$$D = \frac{\sigma_v}{\alpha_u} \frac{\Gamma(1/r)}{\Gamma(\mu)} \left(\frac{\alpha_u}{r^2 \alpha_\kappa} \right)^{m/r} \tag{2.28}$$

$$E = \frac{r-m}{r} \tag{2.29}$$

The 3-D flux footprint can then be expressed as:

$$f(x, y, z_m) = \frac{1}{\sqrt{2\pi} D x^E} \exp\left[-\frac{y^2}{2(Dx^E)^2} \right] C x^{-A} \exp\left(-\frac{B}{x} \right) \tag{2.30}$$

The first half of the equation is the Gaussian crosswind distribution and the second half is the crosswind-integrated longitudinal distribution. The input parameters for each footprint model along with measurement methods are shown in Table 2.3.

Table 2.3: Footprint model inputs and their respective measurement methods.

□ootprint Inputs	Raw Variables	Measurement Method	Employed by:		
			S90	H2000	KM01
Friction velocity, u_*	u,v,w	CSAT3	Yes	Yes	Yes
Measurement height, z	—	Constant in this study	Yes	Yes	Yes
Zero-plane displacement height, d	h_c, LAI	Field measurements	Yes	Yes	Yes
Roughness length, z_0	z, h_c, LAI, u, v, w	CSAT3, Field meas.	Yes	Yes	No
Monin-Obukhov length, L	z, h_c, LAI, T, u, v, w	CSAT3, Field meas.	Yes	Yes	Yes
Standard deviation of lateral wind, σ_v	v	CSAT3	Yes	Yes	Yes

Footprint Contribution from Each Field

The S90, H2000, and KM01 footprint functions were determined for each hourly flux. This was done by first rotating into the mean wind direction the respective x and y coordinates of a 450 x 420 grid with each point representing one square meter (i.e. the size of the entire four-field site) centered at the position of each EC system. The rotated coordinates then were used to calculate the relative footprint contribution of each point on the grid. The footprint contribution of each field was then found by creating a 450 by 420 matrix for each field that consisted of 1s and 0s with the 1s representing the area of interest; multiplying each of those respective matrices by the matrix of footprint density weights; and then summing all the elements of the final matrix. Matlab codes, following this procedure for each footprint model, are shown in Appendix B and C.

Footprint Validation Procedure

The premise of validating footprint models using water vapor as a natural tracer is that if the footprint model correctly estimates the footprint weight for each element of the heat flux source area then those elemental footprint weights represent a fraction of the EC-derived ET. If then the ET for each element of the heat flux source area can be accurately measured by another method the sum of the products of footprint weights and their respective EC-based ET rates should equal that of the independently measured ET value. Following that premise, the cumulative footprint within each of the fields was used to calculate a composite ET ($ET_{composite}$) which was then compared to the measured ET value at EC8.

$$ET_{composite} = F_{NE} * ET_{EC1} + F_{NW} * ET_{EC3} + F_{SW} * ET_{EC5} + F_{SE} * ET_{EC2} \quad (2.31)$$

where, F is the cumulative footprint fraction for each field (subscripts indicate the field) and ET_{EC1}, ET_{EC3}, ET_{EC5}, and ET_{EC2} are the EC-based ET (mm h^{-1}) from EC1, EC3, EC5, and EC2, respectively.

The underlying assumption is that the surface conditions within each field are homogeneous. In order to ensure that EC-based ET values from each field were representative of the field, an infield cumulative footprint fraction limit was set. The selection of the footprint fraction limit was based on the optimization of excluding data that had significant influence from areas outside of the field while still retaining enough data for analysis. A minimum 80% of the footprint for EC1, EC3, EC5, and EC2 must have come from the NE, NW, SW, and SE fields, respectively.

ET Correction Using Footprint Fractions

When the footprint for a heat flux measurement extends beyond the field of interest the flux is then influenced by the surrounding area heat fluxes. During the summer of 2008 the East fields were irrigated and as a result the ET from those fields was greater than that from the West fields. Therefore, any contribution to the flux from the West fields would be cause for an underestimation of EC-based ET for the East fields. Using the same footprint limit as in the validation procedure, the ET at EC8 was corrected for footprint fraction extending beyond the NE field using the model shown below:

$$\begin{aligned} ET_{FC} = {} & ET_{EC8} + F_{NW}\, dET_{EC3} + F_{SW}\, dET_{EC5} + F_{SE}\, dET_{EC2} \\ & + \left[1 - \left(F_{NE} + F_{NW} + F_{SW} + F_{SE}\right)\right] ET_{EC8} \end{aligned} \quad (2.32)$$

where, ET_{FC} is corrected ET considering footprint and dET_i is the difference in ET between the ith and EC8 systems:

$$dET_i = ET_{EC8} - ET_i \quad (2.33)$$

The contribution from adjacent fields to the ET measured by EC8 is removed by the terms dET_{EC3}, dET_{EC5}, and dET_{EC2}, in Eq. (2.32) while the latter part of the equation removes any contribution to the ET at EC8 that is not accounted for on the adjacent NW, SW, and SE fields based on the assumption that there is little to no ET from the area extending beyond the four fields and thus $dET=ET_{ec8}-0$. The effectiveness of the adjustment was determined by comparing ET_{FC} to ET measurements from the NE lysimeter.

Statistical Analysis

The mean bias error (MBE), the root mean square error (RMSE), and linear regression analysis based on least squares method for comparison of fitted equation slope and intercept were used for the comparison of ET values (Willmott 1982; Willmott et al. 1985).

$$MBE = \frac{1}{N}\sum_{i=1}^{N}\left(P_i - O_i\right) \tag{2.34}$$

where, N is the number of pairs compared, P_i predicted or corrected value and O_i the observed value.

$$RMSE = \sqrt{\frac{1}{N}\sum_{i=1}^{N}\left(P_i - O_i\right)^2} \tag{2.35}$$

Results and Discussion

The grass reference ET, air and soil temperature, precipitation, relative humidity, and growing degree days (GDD) were analyzed to assess the temporal variability of the meteorological conditions during the study period at site EC8 (Figure 2.4). There was a considerable amount of variability in the air and soil temperature early and late in the season with the end of July and beginning of August being the steadiest period of time. There was a significant amount of precipitation in mid-August after which there was a drop in the temperature for the remainder of the season. Crop development is commonly related to GDD which is a measurement of heat energy a plant encounters each day during the growing season. A GDD is calculated from daily maximum and minimum air temperature values:

$$GDD(°C) = \frac{(T_{\max} - T_{\min})}{2} - T_{base} \quad when\ GDD > 0 \tag{2.36}$$

This concept of GDD resulted from observations that plants do not grow below a base temperature (T_{base}). The T_{base} for cotton is 15.6°C (Gowda et al. 2007). The East fields were planted 15 days prior to the West fields and therefore the growth in those fields outpaced that of the West fields. Both East and West fields were in the square initiation stage from July 5-26 and then both were in the flowering growth stage from August 6 through the end of the study period.

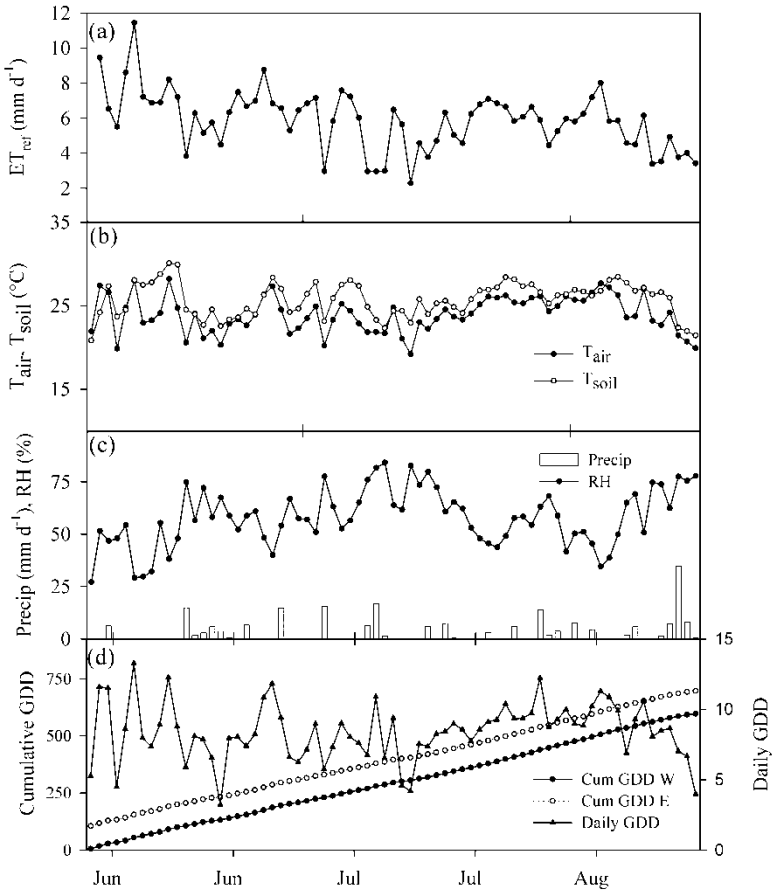

Figure 2.4: Average daily values of the meteorological conditions during the study period. (a) Grass reference ET, (b) air and soil temperature (45 cm), (c) relative humidity [RH] and daily cumulative precipitation, and (d) daily growing degree days [GDD], and cumulative GDD for the East and West fields.

The wind rose plot in Figure 2.5a shows that the wind direction came primarily from the South to South-Southwest direction for the duration of the study. Since the EC systems used to compute $ET_{composite}$ (i.e., EC1, EC2, EC3, EC5) were located at the northeast corner of each field,

the maximum amount of fetch was greatly utilized and thus a representative estimate of ET for each field was obtained. About 87% of the wind velocity, during the research period, was between 0.5 and 5.7 m s^{-1} (Figure 2.5b).

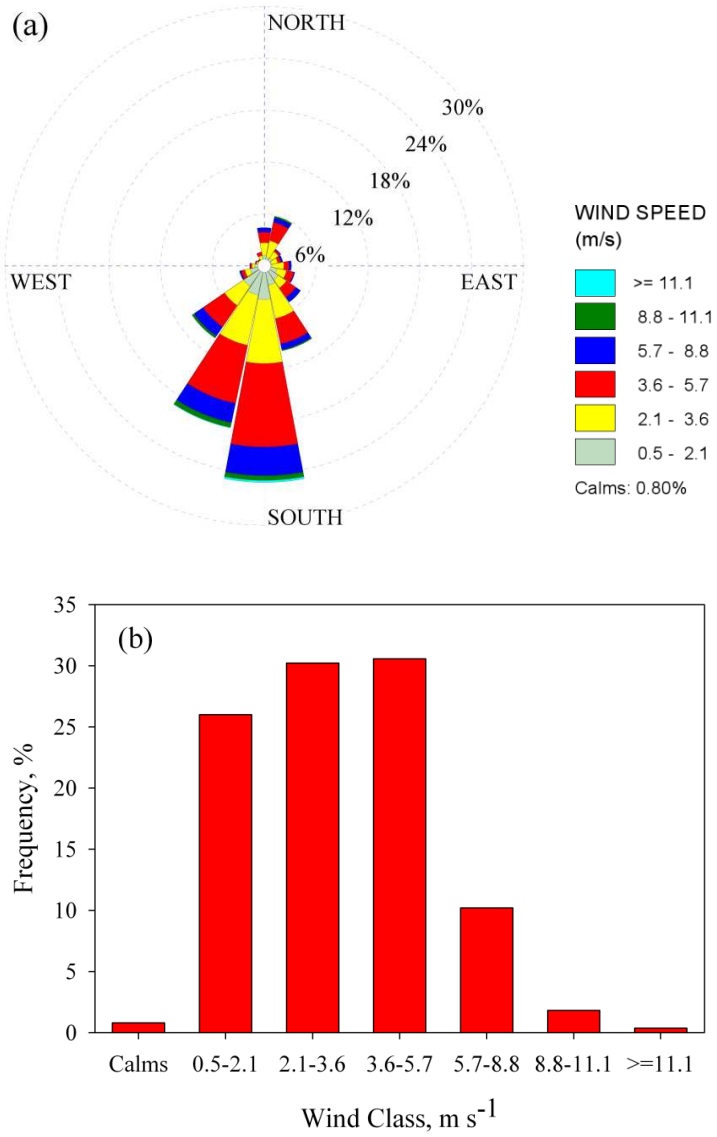

Figure 2.5: Wind rose plot (a) and wind class frequency distribution (b) for June 6 – October 10, 2008 using wind data from EC8.

Surface Roughness

An underlying assumption for all three analytical footprint models presented here is that the surface is spatially homogenous for a virtually infinite distance. This condition is rarely met when measuring fluxes over agricultural lands due to the typical patchwork of fields each with a

different crop, surface roughness, and water availability. Although it is the objective of this study to ascertain the effectiveness of analytical footprint models over such terrain; each field within this study needs to be reasonably homogeneous in order to properly estimate the composite ET. There are many factors that contribute to the spatial variability of a field (e.g., soil type, irrigation system uniformity, topography, soil fertility, plant germination and etc.). However, a good indicator of the combined effect of these conditions is the vegetation. The crop heights for all the fields were similar early in the growing season (<DOY 180) but then began to diverge (Figure 2.6). The East fields were planted earlier and were fully irrigated and thus the cotton grew more in these fields. The North fields showed a taller crop than their respective South fields later in the growing season most likely due to row orientation.

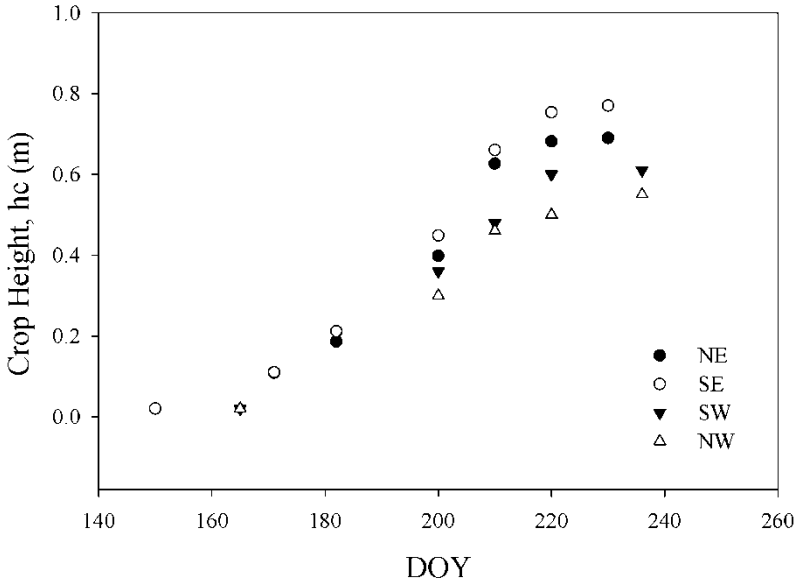

Figure 2.6: Crop height with respect to time (DOY) for the NE, SE, SW, and NW fields.

Though the crop height gives one a general idea of the surface conditions there still can be a considerable amount of variability that goes undetected if not visually inspected. Using remote sensing data, the amount of vegetation cover can be determined using the normalized difference vegetation index (NDVI). The NDVI is calculated from the fraction of visible (VIS) and near-infrared (NIR) light reflected by vegetation and varies from -1 to 1(Kriegler et al. 1969).

The pigment in plant leaves, chlorophyll, strongly absorbs visible light (in the bandwidth 0.4 to 0.7 µm of the electro-magnetic spectrum) for use in photosynthesis. The cell structure of the leaves, on the other hand, strongly reflects near-infrared light (from 0.7 to 1.1 µm). The more leaves a plant has, the more these wavelengths of light are affected, respectively. The formula for calculating NDVI is:

$$NDVI = \frac{NIR - VIS}{NIR + VIS} \tag{2.36}$$

NASA's Landsat 5 thematic mapper satellite operates on a 16-day acquisition schedule in which an image will be captured of any given surface every 16 days. The satellite reflectance images of the site for the stated study period were obtained using the online Earth Explorer tool (Earth Explorer 2011) and NDVI calculations were performed by fellow graduate student Mcebisi Mkhwanazi. Three of the nine images covering the crop growth period could not be used due to excessive cloud cover. The remaining six images are shown in Figure 2.7 (pixel size of 30m x 30m). The vegetative cover was uniform over all fields with a mean NDVI of 0.24 and standard deviation (sd) of 0-0.01(0.0-4.7%) during the period of DOYs 155-171 (Figure 2.8). By DOY 187 the East fields began to show greater vegetation coverage but sd of NDVI within each field remained small at 0.01(2.5%) and 0.02 (4.0%) for the West and East fields, respectively. Variability in NDVI within each field increased significantly by DOY 203 with the North fields showing the greatest relative variability with sd of 0.05 (10.4%) and 0.04 (11.3%) for the NE and NW fields, respectively. The variability in the surface vegetation in the NW field was mostly due to poor seed germination in this field possibly due to chemical residual from previous crop.

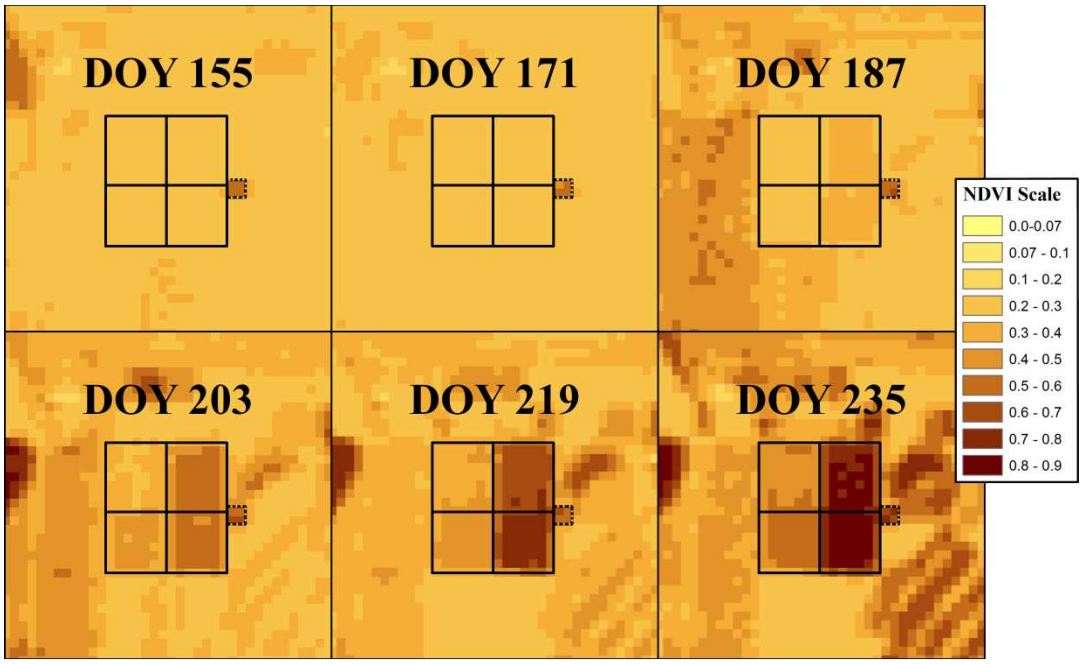

Figure 2.7: NDVI images with lysimeter fields (solid lines) and weather station grass field (dotted lines) boundaries shown for DOYs 155, 171, 187, 203, 219, and 235 derived from reflectance images courtesy of the U.S. Geological Survey.

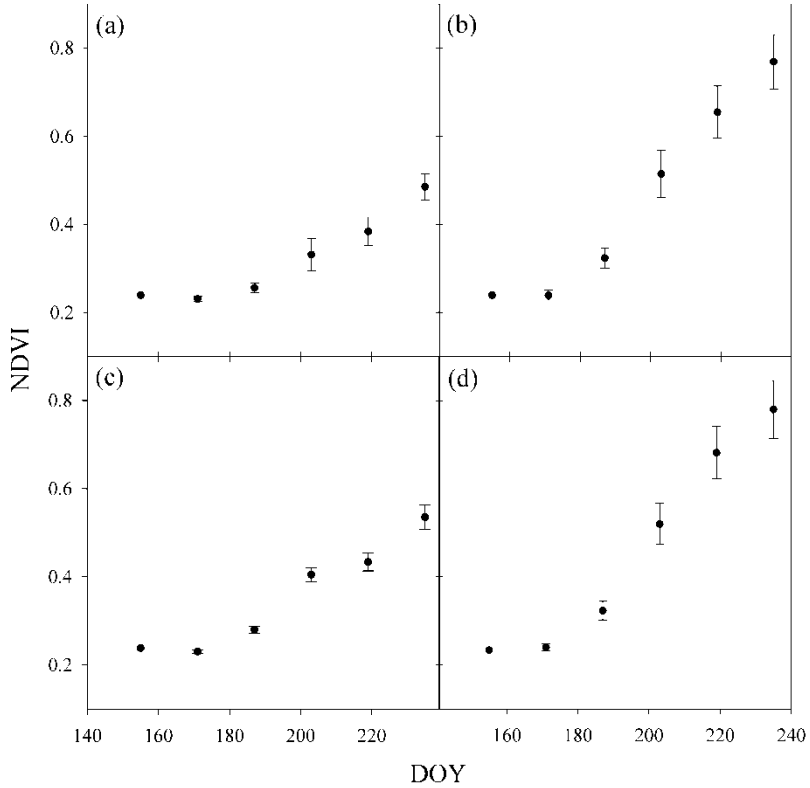

Figure 2.8: Mean NDVI with standard deviation (bars) for (a) NW, (b) NE, (c) SW, and (d) SE fields on DOYs 155, 171, 187, 203, 219, and 235.

Instrument Variability

Prior to field deployment, the nine EC systems used in BEAREX08 were co-located along the edge of an irrigated (center pivot) wheat field so that the instrument response of the EC systems (in relation to each other) could be compared (Alfieri et al. 2011). The results of that analysis showed substantial variability in the uncertainty estimates during advective conditions, but for non-advective daytime periods the mean uncertainty in the measurements of sensible heat and latent heat were approximately 13 W m^{-2} and 27 W m^{-2}, respectively (Alfieri et al. 2011). An infield comparison of LE at EC1 to EC8 under non-advective conditions resulted in a MBE of -26.5 W m^{-2} (-8.57%) and RMSE of 43.0 W m^{-2} (12.56%). The infield comparison of LE at EC2 to EC9 showed an even larger error with MBE of -87.6 W m^{-2} (-20.83%) and RMSE of 103.3 W m^{-2} (24.0%). The validation of the footprint models is directly related to the reliability of the ET estimate for each field. This inconsistency between EC systems make it is difficult to get an accurate $ET_{composite}$ calculation when using several of the EC systems in this study.

Footprint Validation

The statistical results of the comparison of $ET_{composite}$ ET from EC8 are shown in Table 2.4. All three models showed large errors. The cause for such large errors was attributed to the inter-instrument variability of 26.5 ±43.0 W m^{-2} and -87.6±103.3 W m^{-2} for the NE and SE EC systems, respectively. An alternative method was explored in which lysimeter data from the East fields was used to calculate $ET_{composite}$. The SE lysimeter ET was representative of the field ET for the SE field as was the NE lysimeter after correction as shown by Evett et al. (2011b). Since the variability between sensors was found to be significant the $ET_{composite}$ was recalculated using data from the East lysimeters, EC3, and EC5.

Table 2.4: Comparison of composite ET to ET from EC8.

Footprint Model	N	MBE (mm h^{-1})	MBE (%)	RMSE (mm h^{-1})	RMSE (%)	Slope	Intercept (mm h^{-1})	R^2
S90	38	-0.10	-24.45	0.12	16.66	0.68	0.027	0.85
H2000	31	-0.10	-21.60	0.12	15.71	0.64	0.052	0.83
KM01	40	-0.09	-22.09	0.11	15.54	0.69	0.032	0.83

Due to the variability in meteorological and surface conditions with respect to time, the $ET_{composite}$ was evaluated for two separated periods of time. The statistical results of the comparison of $ET_{composite}$ calculated using combination of lysimeter and EC data to ET from EC8 are shown in Table 2.5. During the initial growth stage the surface roughness was uniform but small with an NDVI less than 0.27 and 0.32 for the West and East fields, respectively. The smoother surface and high average wind velocity of 5 m s^{-1} caused the footprints to extend farther upwind than those for later in the study when the surface was rougher and the wind velocity calmer at an average of 3 m s^{-1} (Table 2.6). The minimum cumulative footprint limit caused more data to be filtered out during this early period and thus the reason for less data. Only four data points could be obtained for the S90 model for the early growth stage which is not enough data to draw a good conclusion on its performance during this period of time. However, both H2000 and KM01 showed larger errors during the initial growth stage than they did later in the growing season. As the surface roughness increased with the growth of the crop, the discrepancy between the three models and between $ET_{composite}$ and ET from EC8 narrowed. During the latter period of the study the MBE was -0.03 to -0.04 mm h^{-1} (-3.30% to -4.76%) and RMSE was 0.10 mm h^{-1} (10.19% to 11.39%). For the entire study period all three models performed well with the S90 and H2000 performing slightly better than KM01.

Table 2.5: Comparison of composite ET calculated using combination of lysimeter and EC data to ET from EC8 for different growth stages and the entire study period.

Footprint Model	N	MBE (mm h^{-1})	MBE (%)	RMSE (mm h^{-1})	RMSE (%)	Slope	Intercept (mm h^{-1})	R^2
DOY 158-194								
S90	4	-0.04	-8.04	0.05	7.70	0.71	0.069	0.98
H2000	18	-0.04	-6.08	0.08	10.91	0.60	0.106	0.93
KM01	15	-0.05	-6.27	0.10	11.96	0.58	0.117	0.96
DOY 195-228								
S90	32	-0.03	-3.30	0.10	10.80	0.89	0.048	0.84
H2000	37	-0.03	-3.46	0.10	10.67	0.88	0.053	0.83
KM01	46	-0.04	-4.76	0.10	11.39	0.89	0.038	0.82
DOY 158-228								
S90	36	-0.03	-3.83	0.09	10.50	0.91	0.030	0.87
H2000	55	-0.03	-4.32	0.09	10.75	0.89	0.032	0.88
KM01	61	-0.04	-5.13	0.10	11.54	0.87	0.039	0.85

Table 2.6: Average Kormann and Meixner cumulative footprint (%) for each field during different growth stages and the entire study period.

EC System	Cumulative Footprint				
	NE	SE	NW	SW	Combined
DOY 158-194					
EC8	69	11	1	3	85
EC3	4	1	74	5	83
EC5	0	3	0	76	79
DOY 195-228					
EC8	80	6	1	1	88
EC3	2	1	84	3	90
EC5	0	1	0	85	87
DOY 158-228					
EC8	77	7	1	2	87
EC3	3	1	80	4	87
EC5	0	2	0	82	84

During the early growth stage the surface roughness is very small. Neftel et al. (2008) pointed out that the KM01 uses wind velocity, u, instead of the roughness length, z_0. Under ideal conditions the use of u and z_0 are equivalent since they are related. The advantage of using u is that it is measured in situ along with the other input parameters where as the z_0 is derived using Monin-Obukhov similarity theory or estimated using empirical relationships with the canopy height. Neftel et al. (2008) also showed that the size of the KM01 footprint was heavily dependent on the ratio of u/u_* which is interpreted as the relative strength of horizontal advection vs. vertical diffusion. As shown in Figure 2.9, the u/u_* was higher during the early growth stage decreasing steadily until about DOY 200 where it mostly leveled off. The higher u/u_* is why the footprint extended farther upwind during the early growth stage and thus the reason why less of the footprint was within the field of interest as shown in Table 2.6.

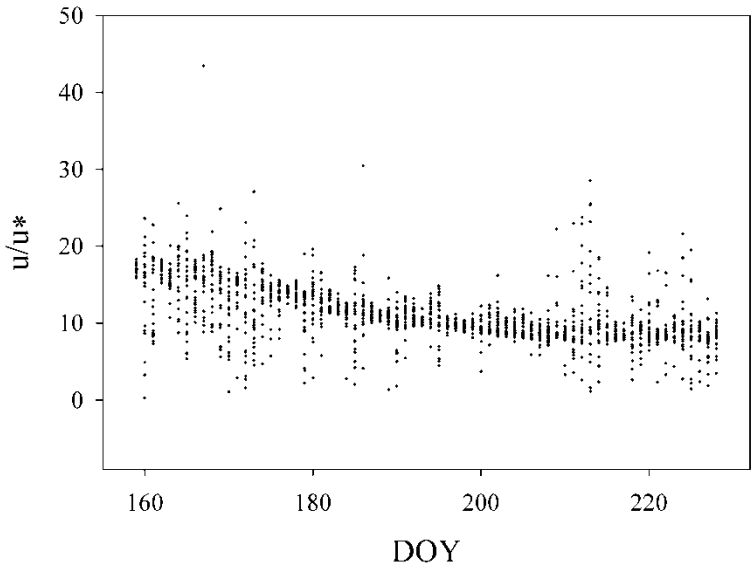

Figure 2.9: The change in the ratio u/u_* over time as the crop canopy develops for NE field.

The difference in each footprint model under both stable and unstable atmospheric conditions is shown in Table 2.7. For the stable condition the S90 performed the best with a MBE of -0.03 mm h^{-1} (-3.16%) and RMSE of 0.12 mm h^{-1} (12.75%). However, Figures 2.10 and 2.11 show that the S90 and KM01 models yielded similar shapes, whereas the H2000 model has a wider and longer overall footprint with a smaller concentration near the tower. For the unstable condition all three models performed similarly and considerably better than the stable condition with RMSE ranging from 0.05 to 0.07 mm h^{-1} (7.20 to 9.13%), which is consistent with the shapes of the footprint illustrated in Figures 2.12 and 2.13. Although it should be noted, all of the models did show strong influence close to the tower, especially for the unstable atmospheric condition. Since a more accurate estimate of the ET was obtained using the lysimeters in the East fields as compared to the West fields in which the EC systems were used, the $ET_{composite}$ for the unstable condition should be more accurate as well.

Table 2.7: Comparison of composite ET calculated using combination of lysimeter and EC data to ET from EC8 for different atmospheric stability regimes.

Footprint Model	N	MBE (mm h^{-1})	MBE (%)	RMSE (mm h^{-1})	RMSE (%)	Slope	Intercept (mm h^{-1})	R^2
Stable								
S90	19	-0.03	-3.16	0.12	12.75	0.85	0.090	0.73
H2000	21	-0.05	-4.36	0.13	14.10	0.77	0.139	0.62
KM01	26	-0.05	-6.32	0.13	14.14	0.85	0.063	0.71
Unstable								
S90	17	-0.03	-4.58	0.05	7.20	0.83	0.057	0.88
H2000	34	-0.03	-4.30	0.05	8.01	0.82	0.048	0.88
KM01	35	-0.03	-4.32	0.07	9.13	0.76	0.077	0.81

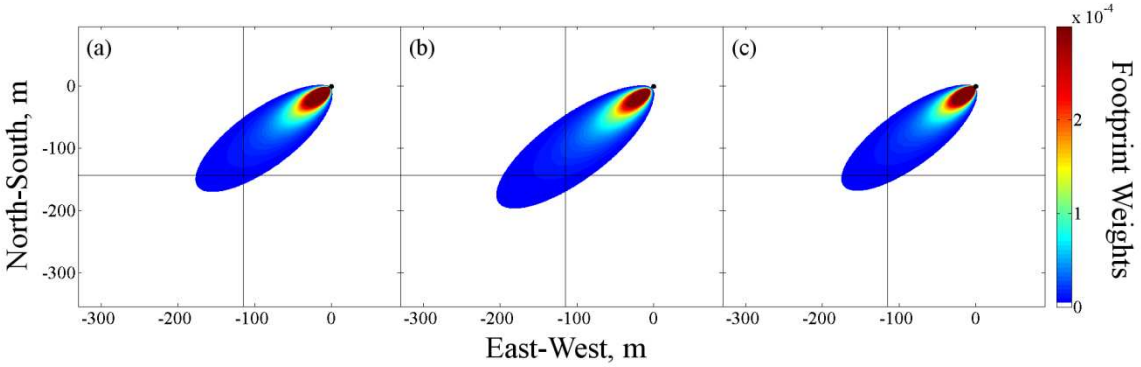

Figure 2.10: Contour plots of footprints at EC1 using S90 (a), H2000 (b), and KM01 (c) models during stable stratification on DOY 218 at 6:30 am CST.

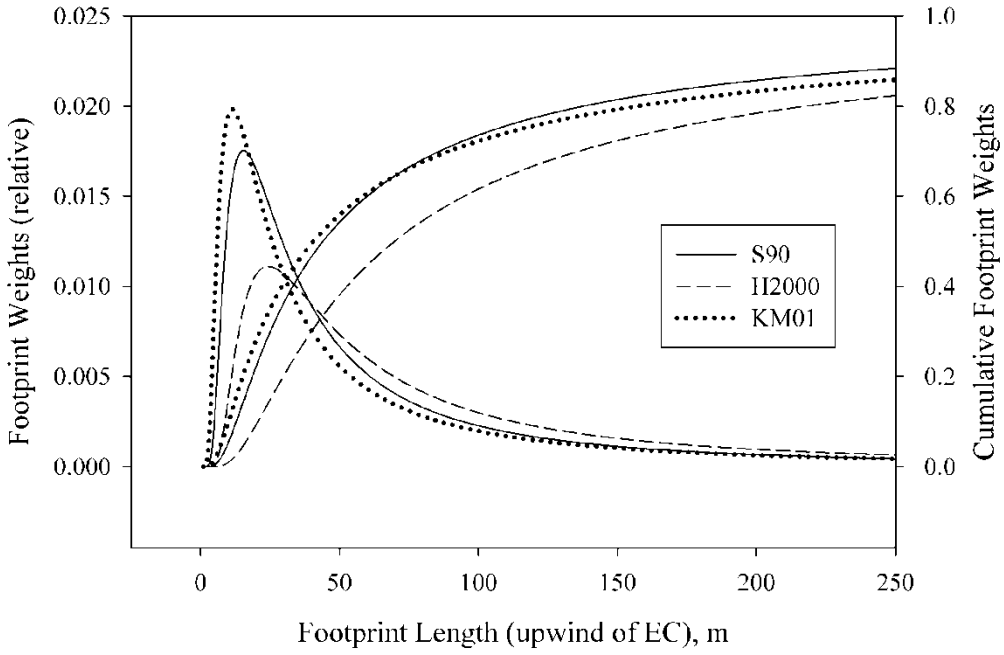

Figure 2.11: One dimensional plot of footprints at EC1 using S90 (a), H2000 (b), and KM01 (c) models during stable stratification on DOY 218 at 6:30 am CST.

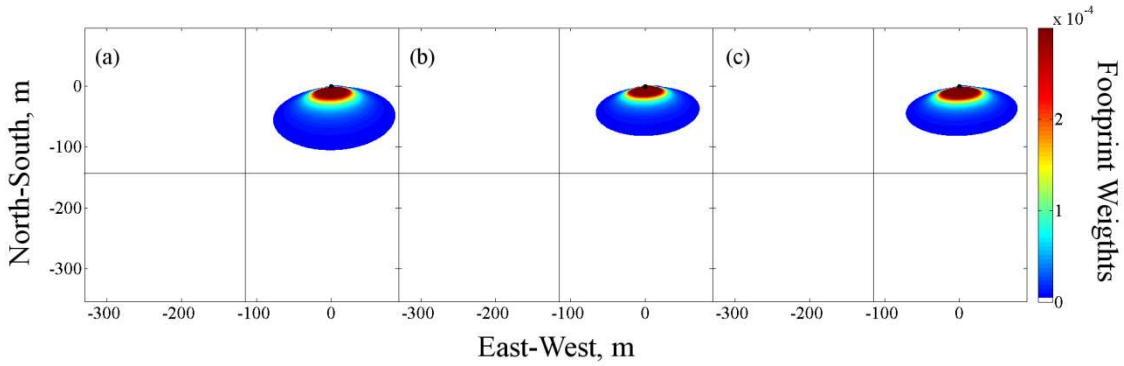

Figure 2.12: Contour plots of footprints at EC1 using S90 (a), H2000 (b), and KM01 (c) models during unstable stratification on DOY 195 at 14:30 am CST.

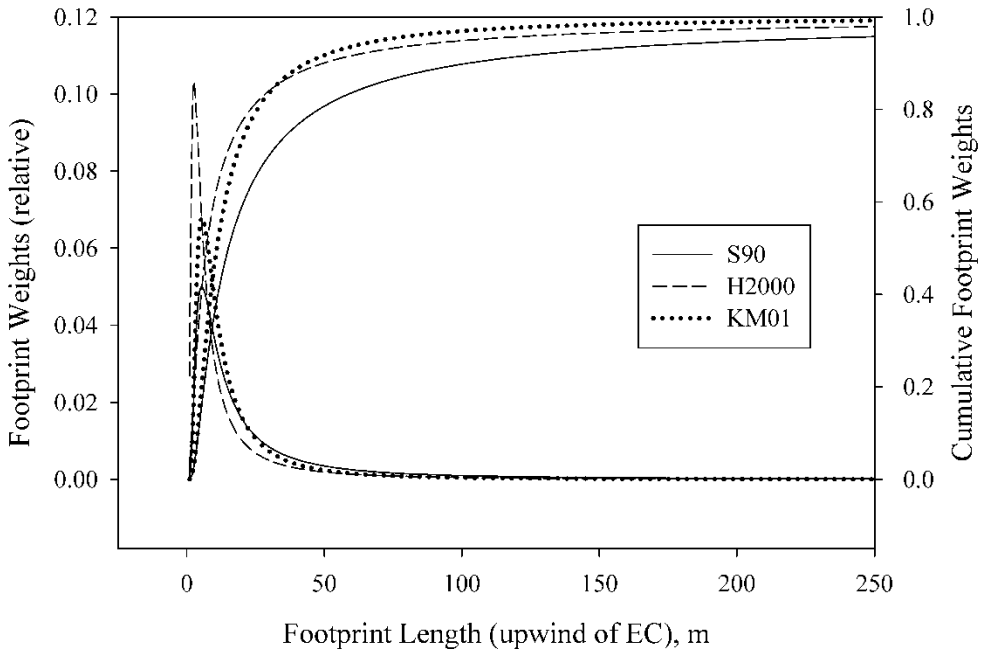

Figure 2.13: One dimensional plot of footprints at EC1 using S90 (a), H2000 (b), and KM01 (c) models during unstable stratification on DOY 195 at 14:30 am CST.

ET Correction Using Footprint Fractions Evaluation

On average 16-30% of the footprint extended beyond the East fields. The EC ET footprint correction, following the procedure outlined in Equation (2.32) was systematically applied to fluxes of good data quality and compared to lysimetric ET rates. As shown in Table

2.8, the footprint corrected EC ET resulted in a MBE of 0.01 mm h^{-1} (0.63%), RMSE of 0.10 mm h^{-1} (11.63%), and slope of 0.99 for KM01. The correction tended to overcorrect during the early growth stage. Each model performed well in correcting EC ET with the S90 and KM01 models performing slightly better than H2000. The results show that area surrounding the field had a significant influence on the heat fluxes measured at site EC8. The EC ET corrected for footprint beyond the area of interest results in a reliable estimate of ET.

Table 2.8: Comparison of footprint corrected ET from EC8 to Lysimeter (NE) ET for different growth stages and the entire study period.

Footprint Model	N	MBE (mm h^{-1})	MBE (%)	RMSE (mm h^{-1})	RMSE (%)	Slope	Intercept (mm h^{-1})	R^2
DOY158-194								
No Ftp Adjustment								
S90	4	-0.04	-10.78	0.04	7.57	1.13	-0.093	0.98
H2000	18	-0.02	-7.85	0.06	10.23	1.30	-0.137	0.92
KM01	15	-0.01	-7.23	0.08	11.65	1.42	-0.189	0.93
Ftp Adjustment								
S90	4	0.02	2.00	0.04	6.04	1.30	-0.108	0.98
H2000	18	0.03	3.47	0.09	12.15	1.50	-0.165	0.92
KM01	15	0.03	4.01	0.10	13.91	1.61	-0.217	0.94
DOY195-228								
No Ftp Adjustment								
S90	21	-0.07	-9.01	0.13	12.84	0.80	0.080	0.84
H2000	25	-0.07	-9.70	0.13	12.73	0.81	0.063	0.85
KM01	28	-0.07	-10.32	0.12	12.59	0.82	0.049	0.85
Ftp Adjustment								
S90	21	0.00	0.59	0.11	11.23	0.92	0.063	0.84
H2000	25	0.00	0.06	0.11	10.83	0.93	0.051	0.85
KM01	28	-0.01	-1.18	0.10	10.20	0.94	0.032	0.86
DOY158-228								
No Ftp Adjustment								
S90	25	-0.07	-9.29	0.12	12.15	0.82	0.056	0.87
H2000	43	-0.05	-8.93	0.11	11.75	0.87	0.027	0.88
KM01	43	-0.05	-9.24	0.11	12.27	0.87	0.025	0.86
Ftp Adjustment								
S90	25	0.01	0.81	0.11	10.58	0.94	0.049	0.87
H2000	43	0.01	1.49	0.10	11.40	0.98	0.025	0.88
KM01	43	0.01	0.63	0.10	11.63	0.99	0.020	0.86

Conclusion

Validation of footprint models is only as accurate as the estimate of the natural tracer (e.g., water vapor flux, ET) for each ground cover condition within the footprint. In this study there was considerable variability in the estimate of ET between EC systems deployed which brought validation procedure into question since errors in footprint estimate and instrument variability could not be differentiated. The $ET_{composite}$ estimated using a combination of EC and lysimeter based ET estimates showed that all three tested "heat flux source area" models accurately estimated the footprint. The footprints extended farther upwind early in the growing season due to the higher relative strength of advection vs. vertical diffusion which is related to the smoother surface when the crop is small. The somewhat larger errors between composite ET and measured ET at EC8 during this early growth stage were probably due to the inaccurate assumption that there was no ET contribution from the fallow land to the West of the study site. The correction of EC based ET considering the footprint fraction that extends beyond the field of interest decreased the absolute MBE by about 8% and the RMSE by about 1%. Each of the three footprint models yielded a good estimate of the footprint over the highly advective and heterogeneous agricultural land of the Texas Panhandle. The H2000 model gave slightly more consistent results across all growth stages and atmospheric stability conditions. Depending on the surface roughness and field dimensions the footprint could be primarily confined within the boundaries of the field. For a cotton field once the crop height and NDVI reaches 0.25 m and 0.3, respectively, then a fetch of 350 m is sufficient to confine more than 80% of the footprint within the field.

It is recommended that care be taken when measuring ET during the early growth stage of a crop when the surface is smoother. An option during this period of time would be to deploy the EC system at a minimum height of two meters which increases the influence of the surface roughness on the turbulence. The system height then could be raised after the initial growth stage. Another option would be to maintain the EC system height but correct ET considering the

footprint which as shown will give a reliable estimate of the ET. The S90, H2000, or KM01 footprint model should be used as a tool to interpret the source area contribution to heat fluxes to an EC system and thus a tool to verify the validity or representativeness of the data. In addition, the correction of EC ET using the proposed model should be used to obtain the most accurate estimate of hourly ET.

CHAPTER 3: EDDY COVARIANCE HEAT FLUX ENERGY BALANCE CLOSURE

Background

The Bushland Evapotranspiration and Agricultural Remote Sensing Experiment 2008 (BEAREX08) was conducted during the 2008 cotton cropping season at the USDA-ARS Conservation and Production Research Laboratory (CPRL), located at Bushland, TX. Researchers from eight federal and state institutions evaluated the ability of land surface energy balance and crop coefficient-based ET models to estimate ET at point, plot, field, and regional scales in a semi-arid, highly advective agricultural region. Instrumentation for the project included aircraft flux and remote sensing, a tethered sonde system, a network of soil moisture, heat flux, and temperature sensors, three Bowen Ratio stations, three large aperture scintillometers, nine EC stations, and four large precision weighing lysimeters (Evett et al. 2011a, 2009).

Site Description

For this study the data from BEAREX08 was used. The geographic coordinates of the CPRL are 35°11'N, 102°06'W, and its elevation is 1,170 m above mean sea level. Soils in and around Bushland are classified as slowly permeable Pullman clay loam. The major crops in the region are corn, sorghum, winter wheat, and cotton. Wind direction is predominantly from the south/southwest direction. The average precipitation that occurs during the cotton growing season (May-October) is 350 mm (Howell et al. 2004). About 600 mm of irrigation, precipitation, and soil water are needed to grow cotton (New 2008), thus irrigation needs to provide about 250 mm of timely water for a successful cotton harvest. The typical growing season grass reference ET is 6.0-8.2 mm day^{-1} (Howell et al. 2004). In addition, the long-term annual microclimatological conditions indicate that the study area is subject to very dry air and

strong winds. Growing season averages at Bushland for air temperature and horizontal wind speed are 20°C and 3.9 m s^{-1}, respectively (Howell et al. 2004).

Large Monolith Weighing Lysimeters

Precision weighing lysimeters (Marek et al. 1988), $3 \times 3 \times 2.3$–m deep, were used to measure cotton ET. Each lysimeter contained a monolithic Pullman clay loam soil core. The lysimeters were located at the center of four fields (210 m East-West by 225 m North-South) two (East) irrigated by a linear move system and two (West) not irrigated. The change in lysimeter mass was measured by load cell (SM-50, Interface, Scottsdale, Ariz.) and recorded by a datalogger (CR7-X, Campbell Scientific Inc., Logan, Utah). The signal was sampled at 0.17 Hz frequency. The high frequency load cell signal was averaged for 5 min and composited to 15-min means. The lysimeter was calibrated as explained in Howell et al. (1995). The lysimeter mass measurement accuracy in water depth equivalent was 0.01 mm, as indicated by the RMSE of calibration. A simple soil water balance using change in water storage from four neutron probes, irrigation, and precipitation data showed that the Northeast (NE) lysimeter had a larger ET than the surrounding field (Evett et al. 2011b). According to that study, the ET measurements from the NE lysimeter were 18% larger than the surrounding field from DOY 182 to 220 due to greater leaf area index (LAI) on the lysimeter than the surrounding field(Evett et al. 2011b). Therefore, the NE lysimeter ET measurements, from that period, were reduced by 18% in order to ensure they were representative of the entire field. Pictures of a lysimeter box and an EC system are shown in Figure 3.1.

Figure 3.1: Lysimeter box with micrometeorological instrumentation (a) and eddy covariance system (b). Photographs courtesy of José Luis Chávez.

Eddy Covariance Energy Balance System

Two EC systems (EC8and EC9) out of the nine from BEAREX08 experiment were used to monitor the exchange of heat fluxes at different parts of the CPRL site. The instrument positions are shown in Figure 3.2. Instrumentation details of all systems used are given in Table 3.1. Time series data consisted of horizontal (u), lateral (v), and vertical (w) wind vectors (m s^{-1}), calculated sonic temperature (T_s, ºC), water vapor concentration (H_2O, g m^{-3}), carbon dioxide concentration (CO_2, mg m^{-3}), and atmospheric pressure (P, kPa), all measured at a frequency of 20 Hz. The CSAT3 sensor was oriented toward the predominant wind direction, with an azimuth angle of 225° from true North for EC8 and 180° for system EC1. Installed within and between the crop rows, about 4 m east from each EC system, were instruments for measuring soil heat flux, soil temperature, and soil volumetric water content. The temperature and water content data were used to calculate soil heat storage in the layer between the surface and the depth of soil heat flux plate installation. Soil heat flux plates (SHFP) were installed at 0.08 m depth within and between crop rows. Soil thermocouple pairs were installed at 0.02 and 0.07 m depths close to the SHFP locations. Soil water content reflectometers (CS616, Campbell Scientific Inc., Logan, UT) were installed slanted at an approximate angle of 13 degrees across the 0.01-0.1 m depth to

measure the volumetric soil water content in this depth zone. Water content reflectometers were field cross-calibrated against water contents reported by a conventional time domain reflectometry (TDR) (TR-100, Dynamax, Inc., Houston, TX) system that used a soil-specific calibration that minimized soil temperature influences on the TDR water contents readings (Evett et al. 2005). Soil temperature was sensed and recorded during the cross-calibration and a soil temperature correction was developed for the CS616 data (Evett and Schwartz 2009).

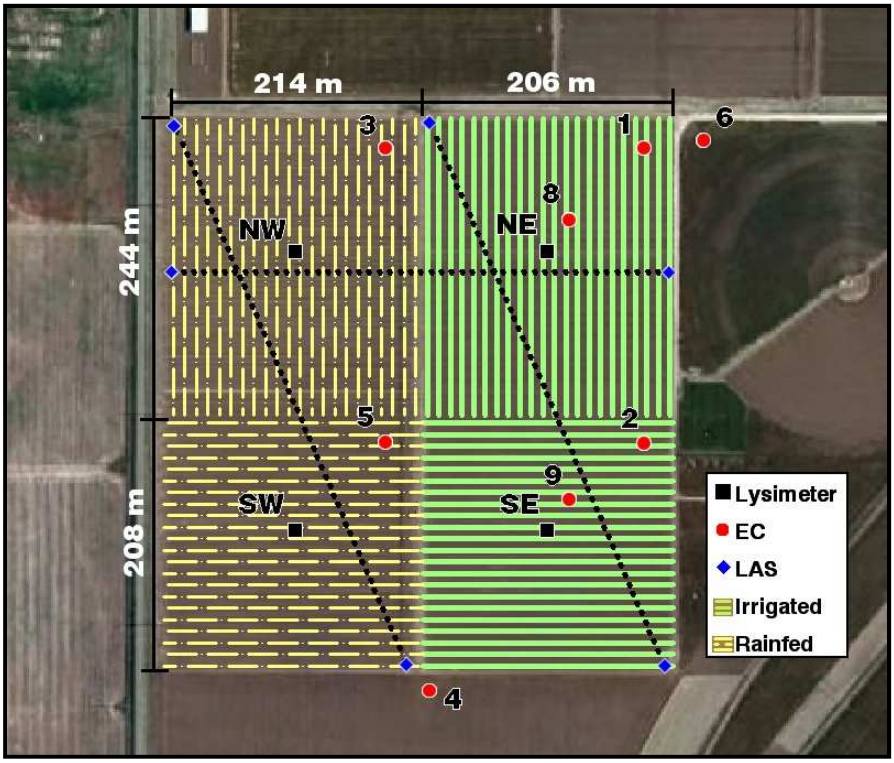

Figure 3.2: Experimental setup at the USDA-ARS, Conservation and Production Research Laboratory, Bushland, TX with the positions of the eddy covariance systems (EC), large weighing lysimeters, and large aperture scintillometers (LAS) and their respective paths (dotted lines) shown. The orientation of the lines corresponds to the orientation of the rows.

Table 3.1: Instrumentation details for eddy covariance systems and lysimeter.

Instrument	EC	Lysimeter
3D Sonic Anemometer	CSAT3[a]	—
Open Path Gas Analyzer	LI-7500[b]	—
Fine Wire Thermocouple	FW05[a]	—
Air Temp/ Relative Humidity	HMP45C[c]	HMP45C[c]
Barometer	CS106[a]	—
Net Radiometer	—	REBS Q*7.1[d], K&Z CM14[e], K&Z CGR3[e]
Soil Heat Flux Plates	(2) REBS HFT-3[d]	(4) REBS HFT-1.1[d]
Soil Temperature	(4) TCAV[a]	(8) TMTSS-020G-6[f]
Soil Water Content	(2) CS616[a]	—
Precipitation Gauge	—	Qualimetrics 6011B[g]
Datalogger	CR3000[a]	CR7X[a]
CSAT Azimuth	225°	—
Measurement Height	2.5 m	—
Sampling frequency	20 Hz[g]	0.17 Hz

Eddy Covariance Data Processing

Time series, high frequency, EC data were post-processed with the EdiRe software package (Clement 1999) following the guidelines described in Lee et al. (2004) and Burba and Anderson (2010) as detailed in Table 3.2. EdiRe is a fast and flexible software tool that allows rapid redesign of routines to enhance question/answer cycle of data analysis. Before covariances were calculated, spikes of six standard deviations from the population mean were removed from the time series. If four or more consecutive data points were detected with values larger than standard deviation then they were not considered as a spike (Vickers and Mahrt 1997). Time delay between the CSAT3 and LI-7500 was removed using a cross-correlation analysis (McMillen 1988). Although the terrain for the site was practically flat, the CSAT3 cannot be perfectly leveled, such that the vertical component (w) is perpendicular to the mean streamline plane. For this reason, the coordinates were rotated using the double rotation method (Kaimal and Finnigan 1994). According to Lee et al. (2004) this method is suitable for ideal sites with little

slope and fair weather conditions. The effects of density fluctuations induced by heat fluxes on the measurement of eddy fluxes of water vapor using the LI-7500 were corrected using the procedure outlined by Webb et al. (1980). Spectral loss in the high frequency band due to path-length averaging, sensor separation, and signal processing was corrected after Moore (1986). Data from the fine wire thermocouple was intermittent due to equipment failure and thus sonic temperature (T_s) was used in sensible heat flux calculation. Schotanus et al. (1983) recommended correcting T_s for crosswind and humidity effects, commonly referred to as the heat flux correction. The CSAT3 implements the crosswind correction online and therefore the heat flux only needed to be corrected for humidity fluctuations. The sonic temperature flux $\overline{w'T_s'}$ was converted to actual temperature flux $\overline{w'T'}$ following the method of Schotanus et al. (1983).

A dimensionless parameter that characterizes the processes in the surface layer is the atmospheric stability parameter (ζ), Eq. (2.2), which is the ratio of the convective production to the mechanical production of turbulent kinetic energy (Campbell and Norman 1998):

$$\zeta = -\frac{0.4 z_m g H}{(T + 273.15)\rho_a C_p u_*^3} \tag{3.1}$$

where, z_m is the horizontal wind speed observation height above the zero-plane displacement height (i.e., z_m=z-d), g is the gravitational acceleration (9.8 m s^{-2}), u_* is the friction velocity (m s^{-1}) and H, T, ρ_a, and C_p are as defined above. Positive ζ represents a stable stratification, negative ζ represents an unstable stratification, and $|\zeta|$<0.02 represents a neutral stratification.

Table 3.2: Post-processing procedure using the software package EdiRe.

Procedure		EdiRe Commands
1	Extract raw time series data	Extract
2	Calculate wind direction	Wind direction
3	Remove spikes	Despike
4	Calculate and remove lag between instruments	Cross correlate, Remove lag
5	Rotate coordinates	Rotation coefficients, Rotation
6	Calculate means, standard deviations, skewness, and kurtosis	1 chn statistics
7	Calculate covariances and fluxes	Latent heat of evaporation, Sensible heat flux coefficient, 2 chn statistics
8	Calculate friction velocity and stability	User defined, Stability - Monin Obukhov
9	Calculate and apply frequency response corrections	Frequency response
10	Calculate and apply Schotanus H correction	Sonic T - heat flux correction
11	Calculate and apply WPL correction	Webb correction
12	Iterate steps 8-11 two times	
13	Convert LE to ET (mm h^{-1})	User defined
14	Calculate roughness length	Roughness length (z_0)
15	Calculate stationarity	Stationarity

The canopy heights (h_c, m) and leaf area index (LAI, m^2 m^{-2}) for the NE and Southeast (SE) fields were measured five times during the study on the following days of the year (DOY): 171, 182, 200, 210, and 220. Crop emergence occurred on DOY 150. Curves were fitted to h_c vs. DOY and LAI vs. DOY data to determine the h_c and LAI as functions of the DOY. The analytical expression from Raupach (1992, 1994; 1995) was used to estimate the zero-plane displacement height (d, m).

$$d = h_c - h_c\left[\frac{1-\exp\left(-\sqrt{c_{d1}\Lambda}\right)}{\sqrt{c_{d1}\Lambda}}\right] \tag{3.2}$$

where, c_{d1} is an empirical constant estimated from laboratory and field data to be on the order of 7.5 (Raupach 1994) and Λ is the canopy area index which for unstressed, growing canopies is equivalent to LAI.

Quality control criteria were set for wind direction, footprint, stationarity, and integral turbulence characteristics. Flow from behind the sensor can be distorted by the instrumentation.

Therefore, any data with a wind direction beyond ±90° of the orientation of the sonic anemometer were excluded from further analysis. The footprint model developed by Kormann and Meixner (2001) was used to calculate the cumulative footprint within the respective field of each EC system and any data with a cumulative footprint less than 80% was excluded from further analysis.

Estimates of fluxes via the eddy covariance method are based on simplified forms of the Navier-Stokes equations for certain atmospheric conditions (Stull 1988). These conditions are not always met and therefore must be evaluated. Tests for stationarity and integral turbulence were performed following methods outlined in Foken and Wichura (1996) and Thomas and Foken (2002). For the stationarity test, covariances between the vertical wind speed (w) and the horizontal wind speed (u) and the air temperature (T) and water vapor (q) scalars for the averaging period of 60-min were compared to covariances of consecutive 5-min intervals within the same period. The periods where deviations, Δ_{st}, were greater than 30% were considered unstationary and excluded from the study:

$$\Delta_{st} = \frac{100\left|\overline{w'x'_5} - \overline{w'x'_{60}}\right|}{\overline{w'x'_{60}}} \tag{3.3}$$

where, x is u for momentum flux and the scalar of interest (T or q) for scalar fluxes and *5* and *60* are subscripts for the 5-min and 60-min covariances, respectively. Integral turbulence tests are used to determine if the turbulence is well developed. With weak turbulence the measuring methods based on surface layer similarities may not be valid (Foken et al. 2004). The integral turbulence test was done by comparing measured similarity functions ($\varphi_{measured}$) for vertical wind speed (φ_w) and temperature (φ_T) with modeled functions (φ_{model}) shown in Table 1 of Thomas and Foken (2002).

$$\varphi_w = \frac{\sigma_w}{u_*} \tag{3.4}$$

$$\varphi_T = \frac{\sigma_T}{T_*} \tag{3.5}$$

where, σ_w and σ_T are the standard deviations of w and T, respectively, and T_* is the dynamic temperature (°C). Any periods with deviations between measured and modeled similarity functions, Δ_{ITT}, greater than 30% were excluded:

$$\Delta_{ITT} = \frac{100\left|\varphi_{\mathrm{mod}\,el} - \varphi_{measured}\right|}{\varphi_{\mathrm{mod}\,el}} \tag{3.6}$$

Bowen Ratio Closure

The lack of energy balance closure is the one of many issues with the EC system. Many researchers are working to find physics based solutions to this issue. In the meantime many are using the EC system to estimate ET and therefore should consider energy balance closure techniques in order to get a more reliable estimate of ET. Twine et al. (2000) discussed how to close the energy balance but it still remains to identify the most appropriate time to apply the closure technique. The simplest and most convenient technique is to ignore all other corrections and simply close the energy balance on energy fluxes calculated from raw data. The problem with this method is that it ignores the fact that the corrections schemes sited in the literature potentially may alter the Bowen ratio (*BR*).

$$BR = H/LE \tag{3.7}$$

The lack of energy balance closure can be quantified as:

$$D = (R_n - G) - (H + LE) \tag{3.8}$$

where D is the EB discrepancy (W m^{-2}). Two methods for closing the energy balance were employed. The first was to assume that H was accurately measured by the EC system and then apply the entire D towards the LE (thus forcing EB closure). This method is hereafter referred to as the LE closure method (LEC). The second method is to assume that the BR is measured correctly by the EC system and adjust both H and LE while conserving the BR. Both of these

methods were applied before and after the stated corrections for times steps that had a R_n-G>200 W m^{-2} in order to avoid problematic nighttime and transition periods of the day.

Results and Discussion

The energy balance closure methods were evaluated for two growth stages and the entire study period by comparing EC8 and EC9 ET to ET from the NE and SE lysimeters, respectively, as shown in Tables 3.3 and 3.4. The MBE and RMSE for uncorrected EC ET was -0.08 mm h^{-1} (-15.88%) ± 0.12 mm h^{-1} (16.40%) for EC8 and -0.19 mm h^{-1} (-28.08%) ± 0.23 mm h^{-1} (26.21%) for EC9. The application of the EdiRe corrections improved the agreement between the EC systems and the lysimeters by similar magnitude with a decrease in the absolute MBE of 0.06 mm h^{-1} (12.46%) and 0.07 mm h^{-1} (12.54%) for EC8 and EC9, respectively. The combination of EdiRe based corrections (coordinate rotation, density, spectral attenuation, and sonic temperature heat flux) and energy balance closure consistently resulted in an overestimation of the ET on the magnitude of 0.02 to 0.08 mm h^{-1} (3.9 to 24.0%). The application of energy balance closure without EdiRe corrections resulted in the smallest errors of ET. It makes more sense to apply the EdiRe corrections since they are based on well established theory, but the results of this study show that applying closure without these corrections yields more accurate results. The BRC method performed well in both growth stages for EC9 with a MBE of -0.02 mm h^{-1} (-0.79%) and RMSE of 0.12 mm h^{-1} (13.64%) for the entire study period. The LEC and BRC methods performed similarly with the exception of the early growth stage for the EC9 where the application of LEC without any other correction resulted in a MBE of 0.07 mm h^{-1} (23.78%) and a RMSE of 0.09 mm h^{-1} (16.25). The difference between these two methods was not significant enough to recommend the application of one method over the other.

Table 3.3: Evaluation of latent heat flux and Bowen ratio energy balance closure with and without common corrections for coordinate rotation, density, spectral attenuation, and heat flux correction by comparing EC8 ET to NE lysimeter ET with significant errors in bold face type.

Footprint Model	N	MBE ($mm\ h^{-1}$)	MBE (%)	RMSE ($mm\ h^{-1}$)	RMSE (%)	Slope	Intercept ($mm\ h^{-1}$)	R^2
DOY 158-194								
No Correction	65	**-0.06**	**-15.65**	**0.10**	**16.46**	0.89	-0.016	**0.66**
EdiRe[a]	65	-0.01	-0.51	0.09	13.79	0.93	0.020	**0.68**
LEC[b]	65	0.02	5.02	0.08	12.61	0.97	0.027	0.73
BRC[c]	65	-0.02	-5.77	0.08	13.15	1.00	-0.020	0.72
EdiRe+LEC	65	0.03	9.66	0.09	14.07	1.03	0.021	0.73
EdiRe+BRC	65	0.02	4.90	0.09	13.21	1.04	0.002	0.73
DOY 195-228								
No Correction	43	**-0.11**	**-16.23**	**0.15**	**16.30**	**0.81**	0.021	0.84
EdiRe[a]	43	-0.05	-7.83	0.11	12.35	**0.84**	0.049	0.84
LEC[b]	43	-0.01	-0.78	0.10	11.02	0.92	0.044	0.85
BRC[c]	43	-0.02	-3.00	0.10	10.80	0.98	-0.004	0.87
EdiRe+LEC	43	0.03	4.72	0.11	11.94	0.98	0.040	0.85
EdiRe+BRC	43	0.03	4.00	0.11	11.88	1.05	-0.004	0.87
DOY 158-228								
No Correction	108	**-0.08**	**-15.88**	**0.12**	**16.40**	**0.83**	0.005	0.84
EdiRe[a]	108	-0.02	-3.42	0.10	13.23	0.86	0.045	0.84
LEC[b]	108	0.01	2.71	0.09	12.01	0.93	0.041	0.87
BRC[c]	108	-0.02	-4.67	0.09	12.27	0.99	-0.016	0.88
EdiRe+LEC	108	0.03	7.69	0.10	13.26	0.99	0.035	0.87
EdiRe+BRC	108	0.02	4.55	0.10	12.70	1.04	0.000	0.88

[a] EdiRe indicates that the correction procedure outline in Table 2 was applied to the fluxes.
[b] LEC indicates that the energy balance discrepancy was applied entirely to the latent heat flux.
[c] BRC indicates that the Bowen ratio energy balance closure was applied to the fluxes.

Table 3.4: Evaluation of latent heat flux and Bowen ratio energy balance closure with and without common corrections for coordinate rotation, density, spectral attenuation, and heat flux correction by comparing EC9 ET to SE lysimeter ET with significant errors in bold face type.

Footprint Model	N	MBE ($mm\ h^{-1}$)	MBE (%)	RMSE ($mm\ h^{-1}$)	RMSE (%)	Slope	Intercept ($mm\ h^{-1}$)	R^2
DOY 158-194								
No Correction	26	**-0.08**	**-17.47**	**0.11**	**17.00**	0.80	0.002	0.83
EdiRe[a]	26	-0.02	0.53	0.08	14.89	0.78	0.070	0.80
LEC[b]	26	**0.07**	**23.78**	**0.09**	**16.25**	0.92	0.104	0.91
BRC[c]	26	0.01	5.27	0.06	11.75	0.98	0.017	0.89
EdiRe+LEC	26	**0.08**	**24.00**	**0.09**	**16.89**	1.00	0.075	0.91
EdiRe+BRC	26	**0.04**	**15.08**	0.08	14.54	1.02	0.038	0.89
DOY 195-228								
No Correction	81	**-0.23**	**-31.49**	**0.26**	**28.54**	**0.65**	0.022	0.82
EdiRe[a]	81	**-0.16**	**-20.70**	**0.19**	**20.62**	**0.74**	0.035	0.83
LEC[b]	81	-0.01	0.82	0.12	13.66	0.83	0.106	0.79
BRC[c]	81	-0.03	-2.73	0.13	14.19	0.88	0.052	0.78
EdiRe+LEC	81	0.02	5.04	0.12	14.17	0.90	0.092	0.80
EdiRe+BRC	81	0.02	3.92	0.13	14.58	0.95	0.051	0.79
DOY 158-228								
No Correction	107	**-0.19**	**-28.08**	**0.23**	**26.21**	**0.63**	0.043	0.84
EdiRe[a]	107	**-0.12**	**-15.54**	**0.17**	**19.39**	**0.70**	0.071	0.85
LEC[b]	107	0.01	6.40	0.11	14.33	0.82	0.124	0.84
BRC[c]	107	-0.02	-0.79	0.12	13.64	0.89	0.049	0.84
EdiRe+LEC	107	0.03	9.65	0.11	14.88	0.89	0.103	0.85
EdiRe+BRC	107	0.02	6.63	0.12	14.57	0.95	0.056	0.84

[a] EdiRe indicates that the correction procedure outline in Table 2 was applied to the fluxes.
[b] LEC indicates that the energy balance discrepancy was applied entirely to the latent heat flux.
[c] BRC indicates that the Bowen ratio energy balance closure was applied to the fluxes.

Conclusion

The corrections to EC fluxes for coordinate rotation, density, spectral attenuation, and sonic temperature heat flux are based on well understood physical processes that distort, misrepresent, and violate underlying assumption in the calculation of heat fluxes. The BRC and LEC methods for closing the energy balance are based on assumptions that are not that well understood. Although, even after correcting the fluxes there still is a gap in the energy budget and an underestimation of ET. Further research is needed and being conducted to find the source of these discrepancy but in the meantime the EC system can still yield reliable estimates of ET if the energy balance is closed by adjusting H and LE heat fluxes. The BRC method yielded a good agreement between EC based and lysimeter ET during the entire study period with a MBE of -0.02 $mm\ h^{-1}$ (-4.67 to -0.79%) and RMSE of 0.09 to 0.11 $mm\ h^{-1}$ (12.27 to 13.64%). However,

the application of the LEC and BRC methods did not improve the accuracy of the EC ET values much more than the application of the EdiRe corrections. Therefore, based on the findings of this study it is best not to close the energy balance, but instead apply correction for coordinate rotation, density, spectral attenuation, and sonic temperature heat flux. Further research is needed to explore the effect of applying energy balance closure after individual corrections.

CHAPTER 4: CONCLUSION

Analytical footprint models are simple to implement and capable of giving a good estimate of the flux source area. Although, the underlying assumption of horizontal homogeneity is often violated the models are still viable when used over agricultural lands. Agricultural lands are spatially heterogeneous due to the typical patchwork of fields of different crops, but within each field the vegetation is very homogeneous and depending on the surface roughness and field dimensions the footprint could be primarily confined within the boundaries of the field. For a cotton field once the crop height and NDVI reaches 0.25 m and 0.3, respectively, then a fetch of 350 m is sufficient to confine more than 80% of the footprint within the field. When the surface roughness is smoother the relative strength of horizontal advection vs. vertical diffusion is higher which results in a larger footprint. One method to overcome this issue would be to install the sensors at a minimum recommended height of two meters early in the season. Since the ratio of u/u_* gradually decreases during the initial growth stage and then levels off for the remainder of the growing season, the adjustment of sensor height would only have to be done one time during this transition period.

The S90, H2000, and KM01 footprint models all performed similarly with an average integrated ET MBE of about -0.03 mm h^{-1} (-4.4%) and RMSE of 0.09 mm h^{-1} (10.9%) when comparing the $ET_{composite}$, calculated using the footprint models' relative weights (fractions) and a combination of EC systems and lysimeter ET data, to EC-based ET at EC8. The proposed correction of EC data for footprint that extends beyond the area of interest increased the EC-based ET to a more reliable estimate. When compared to lysimetric values the corrected hourly ET values showed a decrease in the absolute MBE by 8% and the RMSE by 1%.. For this study,

16-30% of the footprint consistently extended beyond the area of interests. Even though the majority of the footprint is within the field the influence of the surrounding dryland in a semi arid climate can be significant.

The correction of EC heat fluxes for coordinate rotation, density, spectral attenuation, and sonic temperature heat flux are all based on well understood physical processes and decrease on average the underestimation of ET by 12.5±12.5%. The application of either the LEC or BRC method without any other correction in the heat fluxes resulted in the a better agreement of EC ET values to lysimeter ET than the application of these methods after the stated corrections. Further research is needed to explore the effect of applying BRC after each of the stated corrections.

It is recommended that the S90, H2000, or KM01 footprint model should be used as a tool to interpret the source area contribution to heat fluxes to an EC system and thus a tool to verify the validity or representativeness of the data. In addition, the correction of EC ET using the proposed model should be used to obtain the most accurate estimate of hourly ET.

REFERENCES

Alfieri JG, Kustas WP, Prueger JH, Hipps LE, Chávez JL, French AN, Evett SR (2011) Intercomparison of Nine Micrometeorological Stations During the BEAREX08 Field Campaign. Journal of Atmospheric and Oceanic Technology. doi:10.1175/2011jtecha1514.1

Allen RG, Pereira LS, Howell TA, Jensen ME (2011) Evapotranspiration information reporting: I. Factors governing measurement accuracy. Agricultural Water Management 98 (6):899-920. doi:DOI: 10.1016/j.agwat.2010.12.015

Aubinet M, Grelle A, Ibrom A, Rannik Ü, Moncrieff J, Foken T, Kowalski AS, Martin PH, Berbigier P, Bernhofer C, Clement R, Elbers J, Granier A, Grünwald T, Morgenstern K, Pilegaard K, Rebmann C, Snijders W, Valentini R, Vesala T (1999) Estimates of the Annual Net Carbon and Water Exchange of Forests: The EUROFLUX Methodology. In: Fitter AH, Raffaelli DG (eds) Advances in Ecological Research, vol Volume 30. Academic Press, pp 113-175

Beyrich F, Herzog HJ, Neisser J (2002) The LITFASS project of DWD and the LITFASS-98 experiment: The project strategy and the experimental setup. Theoretical and Applied Climatology 73 (1):3-18. doi:10.1007/s00704-002-0690-8

Burba GG, Anderson DJ (2010) A Brief Practical Guide to Eddy Covariance Flux Measurements: Principles and Workflow Examples for Scientific and Industrial Applications. LI-COR Biosciences, Lincoln, USA

Calder KL (1952) Some Recent British Work on the Problem of Diffusion in the Lower Atmosphere. Paper presented at the United States Technical Conference on Air Pollution, New York, October 3, 1952

Campbell GS, Norman JM (1998) An Introduction to Environmental Biophysics. Second edn. Springer, New York

Chávez J, Howell T, Copeland K (2009) Evaluating eddy covariance cotton ET measurements in an advective environment with large weighing lysimeters. Irrigation Science 28 (1):35-50. doi:10.1007/s00271-009-0179-7

Chen B, Black T, Coops N, Hilker T, Trofymow J, Morgenstern K (2009) Assessing Tower Flux Footprint Climatology and Scaling Between Remotely Sensed and Eddy Covariance Measurements. Boundary-Layer Meteorology 130 (2):137-167. doi:10.1007/s10546-008-9339-1

Clement R (1999) EdiRe Data Software. 1.5.0.10 edn. University of Edinburgh, Edinburgh, England

Cooper DI, Eichinger WE, Archuleta J, Hipps L, Kao J, Leclerc MY, Neale CM, Prueger J (2003) Spatial source-area analysis of three-dimensional moisture fields from lidar, eddy covariance, and a footprint model. Agricultural and Forest Meteorology 114 (3-4):213-234. doi:Doi: 10.1016/s0168-1923(02)00175-2

Dyer AJ (1974) A review of flux-profile relationships. Boundary-Layer Meteorology 7 (3):363-372. doi:10.1007/bf00240838

Earth Explorer (2011) U.S. Geological Survey. http://earthexplorer.usgs.gov.

Evett SR, Kustas WP, Gowda P (2009) Overview of BEAREX08, a remote sensing field experiment on ET at field, multi-field and regional scales using measurement sand models [abstract]. Paper presented at the American Society of Agronomy, Crop Science Society of America, Soil Science Society of America 2009 Annual Meeting, Pittsburgh, Pennsylvania, November 1-5, 2009

Evett SR, Kustas WP, Gowda P (2011a) Overview of the Bushland Evapotranspiration (ET) and Agricultural Remote Sensing Experiment 2008 (BEAREX08): A remote sensing field experiment evaluating model and measurement techniques quantifying ET at the canopy, sub-field, multi-field and at regional scales. Submitted to Advance in Water Resources

Evett SR, Schwartz RC (2009) Report to BEAREX08 users of CS616 soil water sensor data: Correction algorithm.

Evett SR, Schwartz RC, Howell TA, Baumhardt RL, Copeland KS (2011b) Did weighing lysimeter ET represent surround field ET determined by neutron probe soil water balance for BEAREX08? Submitted to Advance in Water Resources

Evett SR, Tolk JA, Howell TA (2005) Time Domain Reflectometry Laboratory Calibration in Travel Time, Bulk Electrical Conductivity, and Effective Frequency. Vadose Zone Journal 4 (4):1020-1029. doi:10.2136/vzj2005.0046

Foken T (2008) The Energy Balance Closure Problem: An Overview. Ecological Applications 18 (6):1351-1367

Foken T, Gockede M, Mauder M, Mahrt L, Amiro BD, Munger JW (2004) Post-field Data Quality Control. In: Lee X, Massman W, Law B (eds) Handbook of Micrometeorology: A Guide for Surface Flux Measurement and Analysis. Kluwer, Dordrecht, pp 181-208

Foken T, Leclerc MY (2004) Methods and limitations in validation of footprint models. Agricultural and Forest Meteorology 127 (3-4):223-234. doi:DOI: 10.1016/j.agrformet.2004.07.015

Foken T, Wichura B (1996) Tools for quality assessment of surface-based flux measurements. Agricultural and Forest Meteorology 78 (1-2):83-105. doi:Doi: 10.1016/0168-1923(95)02248-1

Gash JHC (1986) A note on estimating the effect of a limited fetch on micrometeorological evaporation measurements. Boundary-Layer Meteorology 35 (4):409-413. doi:10.1007/bf00118567

Gowda PH, Baumhardt RL, Esparza AM, Marek TH, Howell TA (2007) Suitability of Cotton as an Alternative Crop in the Ogallala Aquifer Region. Agron J 99 (6):1397-1403. doi:10.2134/agronj2006.0275

Hammerle A, Haslwanter A, Schmitt M, Bahn M, Tappeiner U, Cernusca A, Wohlfahrt G (2007) Eddy covariance measurements of carbon dioxide, latent and sensible energy fluxes above a meadow on a mountain slope. Boundary-Layer Meteorology 122 (2):397-416. doi:10.1007/s10546-006-9109-x

Hoffman GJ, Evans RG, Jensen ME, Martin DL, Elliot RL (2007) Design and Operation of Farm Irrigation Systems. 2nd edn. ASABE, St. Joseph, MI

Howell TA, Evett SR, Tolk JA, Schneider AD (2004) Evapotranspiration of Full-, Deficit-Irrigated, and Dryland Cotton on the Northern Texas High Plains. Journal of Irrigation and Drainage Engineering 130 (4):9. doi:10.1061/(ASCE)0733-9437(2004)130:4(277) (9 pages)

Howell TA, Schneider AD, Dusek DA, Marek TH, Steiner JL (1995) Calibration and scale performance of Bushland weighing lysimeters. Trans ASAE 38:1018-1025

Hsieh C-I, Katul G, Chi T-w (2000) An approximate analytical model for footprint estimation of scalar fluxes in thermally stratified atmospheric flows. Advances in Water Resources 23 (7):765-772. doi:Doi: 10.1016/s0309-1708(99)00042-1

Kaimal J, Finnigan J (1994) Atmospheric Boundary Layer Flows: Their Structure and Measurement. Oxford University Press, New York

Kenny JF, Barber NL, Hutson SS, Linsey KS, Lovelace JK, Maupin MA (2009) Estimated use of water in the United States in 2005: U.S. Geological Survey Circular 1344.

Kljun N, Kormann R, Rotach MW, Meixner FX (2003) Comparison of the Langrangian footprint model LPDM-B with an analytical footprint model.

Kormann R, Meixner F (2001) An Analytical Footprint Model For Non-Neutral Stratification. Boundary-Layer Meteorology 99 (2):207-224. doi:10.1023/a:1018991015119

Kriegler F, Malila W, Nalepka R, Richardson W Preprocessing transformations and their effects on multispectral recognition. In: Proceedings of Sixth International Symposium on Remote Sensing of Environment, University of Michigan, Ann Arbor, Michigan, 1969. pp 97-131

Leclerc MY, Thurtell GW (1990) Footprint prediction of scalar fluxes using a Markovian analysis. Boundary-Layer Meteorology 52 (3):247-258. doi:10.1007/bf00122089

Lee X, Massman W, Law B (2004) Handbook of Micrometeorology: A Guide for Surface Flux Measurement and Analysis. Kluwer, Dordrecht

Li F, Kustas WP, Anderson MC, Prueger JH, Scott RL (2008) Effect of remote sensing spatial resolution on interpreting tower-based flux observations. Remote Sensing of Environment 112 (2):337-349. doi:10.1016/j.rse.2006.11.032

Mahrt L (1998) Flux Sampling Errors for Aircraft and Towers. Journal of Atmospheric and Oceanic Technology 15 (2):416-429. doi:doi:10.1175/1520-0426(1998)015<0416:FSEFAA>2.0.CO;2

Marcolla B, Cescatti A (2005) Experimental analysis of flux footprint for varying stability conditions in an alpine meadow. Agricultural and Forest Meteorology 135 (1-4):291-301. doi:DOI: 10.1016/j.agrformet.2005.12.007

Marek TH, Schneider AD, Howell TA, Ebeling LL (1988) Design and Construction of Large Weighing Monolithic Lysimeters. Trans ASAE 31 (2):477-484

Mauder M, Foken T (2011) TK3. University of Bayreuth, Bayreuth, Germany

Mauder M, Jegede OO, Okogbue EC, Wimmer F, Foken T (2007) Surface energy balance measurements at a tropical site in West Africa during the transition from dry to wet season. Theoretical and Applied Climatology 89 (3):171-183. doi:10.1007/s00704-006-0252-6

McMillen RT (1988) An eddy correlation technique with extended applicability to non-simple terrain. Boundary-Layer Meteorology 43 (3):231-245. doi:10.1007/bf00128405

Moore CJ (1986) Frequency response corrections for eddy correlation systems. Boundary-Layer Meteorology 37 (1):17-35. doi:10.1007/bf00122754

Neftel A, Spirig C, Ammann C (2008) Application and test of a simple tool for operational footprint evaluations. Environmental Pollution 152 (3):644-652. doi:10.1016/j.envpol.2007.06.062

New L (2008) AgriPartner Irrigation Result Demonstrations 2007. Texas Cooperative Extension Service, Texas A&M University,

Oncley S, Foken T, Vogt R, Kohsiek W, DeBruin H, Bernhofer C, Christen A, Gorsel E, Grantz D, Feigenwinter C, Lehner I, Liebethal C, Liu H, Mauder M, Pitacco A, Ribeiro L, Weidinger T (2007) The Energy Balance Experiment EBEX-2000. Part I: overview and energy balance. Boundary-Layer Meteorology 123 (1):1-28. doi:10.1007/s10546-007-9161-1

Ortega-Farias S, Olioso A, Antonioletti R, Brisson N (2004) Evaluation of the Penman-Monteith model for estimating soybean evapotranspiration. Irrigation Science 23 (1):1-9. doi:10.1007/s00271-003-0087-1

Pasquill F (1974) Atmospheric Diffusion. 2nd edn. J. Wiley & Sons, New York

Rannik Ü, Aubinet M, Kurbanmuradov O, Sabelfeld KK, Markkanen T, Vesala T (2000) Footprint Analysis For Measurements Over A Heterogeneous Forest. Boundary-Layer Meteorology 97 (1):137-166. doi:10.1023/a:1002702810929

Raupach MR (1992) Drag and drag partition on rough surfaces. Boundary-Layer Meteorology 60 (4):375-395. doi:10.1007/bf00155203

Raupach MR (1994) Simplified expressions for vegetation roughness length and zero-plane displacement as functions of canopy height and area index. Boundary-Layer Meteorology 71 (1):211-216. doi:10.1007/bf00709229

Raupach MR (1995) Corrigenda. Boundary-Layer Meteorology 76 (3):303-304. doi:10.1007/bf00709356

Rogiers N, Eugster W, Furger M, Siegwolf R (2005) Effect of land management on ecosystem carbon fluxes at a subalpine grassland site in the Swiss Alps. Theoretical and Applied Climatology 80 (2):187-203. doi:10.1007/s00704-004-0099-7

Saito M, Miyata A, Nagai H, Yamada T (2005) Seasonal variation of carbon dioxide exchange in rice paddy field in Japan. Agricultural and Forest Meteorology 135 (1-4):93-109. doi:10.1016/j.agrformet.2005.10.007

Schmid HP (1994) Source areas for scalars and scalar fluxes. Boundary-Layer Meteorology 67 (3):293-318. doi:10.1007/bf00713146

Schmid HP (1997) Experimental design for flux measurements: matching scales of observations and fluxes. Agricultural and Forest Meteorology 87 (2-3):179-200. doi:Doi: 10.1016/s0168-1923(97)00011-7

Schmid HP (2002) Footprint modeling for vegetation atmosphere exchange studies: a review and perspective. Agricultural and Forest Meteorology 113:159-183. doi:10.1016/s0168-1923(02)00107-7

Schmid HP, Oke TR (1990) A model to estimate the source area contributing to turbulent exchange in the surface layer over patchy terrain. Quarterly Journal of the Royal Meteorological Society 116 (494):965-988. doi:10.1002/qj.49711649409

Schotanus P, Nieuwstadt FTM, Bruin HAR (1983) Temperature measurement with a sonic anemometer and its application to heat and moisture fluxes. Boundary-Layer Meteorology 26 (1):81-93. doi:10.1007/bf00164332

Schuepp PH, Leclerc MY, MacPherson JI, Desjardins RL (1990) Footprint prediction of scalar fluxes from analytical solutions of the diffusion equation. Boundary-Layer Meteorology 50 (1):355-373. doi:10.1007/bf00120530

Stull R (1988) An Introduction to Boundary Layer Meteorology. Kluwer, Dordrecht

Thomas C, Foken T Re-evaluation of Integral Turbulence Characteristics and their Parameterisations. In: 15th Symposium on Boundary Layers and Turbulence, 2002. Am. Meteorol. Soc. doi:citeulike-article-id:3716256

Thomson DJ (1987) Criteria for the selection of stochastic models of particle trajectories in turbulent flows. Journal of Fluid Mechanics 180:529-556. doi:doi:10.1017/S0022112087001940

Timmermans WJ, Bertoldi G, Albertson JD, Olioso A, Su Z, Gieske ASM (2008) Accounting for atmospheric boundary layer variability on flux estimation from RS observations.

International Journal of Remote Sensing 29 (17-18):5275-5290. doi:10.1080/01431160802036383

Twine TE, Kustas WP, Norman JM, Cook DR, Houser PR, Meyers TP, Prueger JH, Starks PJ, Wesely ML (2000) Correcting eddy-covariance flux underestimates over a grassland. Agricultural and Forest Meteorology 103 (3):279-300. doi:Doi: 10.1016/s0168-1923(00)00123-4

Vesala T, Kljun N, Rannik Ü, Rinne J, Sogachev A, Markkanen T, Sabelfeld K, Foken T, Leclerc MY (2008) Flux and concentration footprint modelling: State of the art. Environmental Pollution 152 (3):653-666. doi:DOI: 10.1016/j.envpol.2007.06.070

Vickers D, Mahrt L (1997) Quality control and flux sampling problems for tower and aircraft data. J Atmos Oceanic Tech 14:512-526. doi:citeulike-article-id:3716279

Webb EK, Pearman GI, Leuning R (1980) Correction of flux measurements for density effects due to heat and water vapour transfer. Quarterly Journal of the Royal Meteorological Society 106:85-100

Willmott CJ (1982) Some Comments on the Evaluation of Model Performance. Bulletin of the American Meteorological Society 63 (11):1309-1313. doi:doi:10.1175/1520-0477(1982)063<1309:SCOTEO>2.0.CO;2

Willmott CJ, Ackleson SG, Davis RE, Feddema JJ, Klink KM, Legates DR, O'Donnell J, Rowe CM (1985) Statistics for the Evaluation and Comparison of Models. J Geophys Res 90 (C5):8995-9005. doi:10.1029/JC090iC05p08995

Wilson K, Goldstein A, Falge E, Aubinet M, Baldocchi D, Berbigier P, Bernhofer C, Ceulemans R, Dolman H, Field C, Grelle A, Ibrom A, Law BE, Kowalski A, Meyers T, Moncrieff J, Monson R, Oechel W, Tenhunen J, Valentini R, Verma S (2002) Energy balance closure at FLUXNET sites. Agricultural and Forest Meteorology 113 (1-4):223-243. doi:Doi: 10.1016/s0168-1923(02)00109-0

APPENDIX A: EDIRE PROCESSING LIST FOR EC8

```
Set Values
        From Time =
        To Time =
        Number of Variables = 10
        Storage Label = z
        Assignment value = 2.5
        Storage Label = CSATSclrPL
        Assignment value = 0.1155
        Storage Label = LiCor7500PL
        Assignment value = 0.125
        Storage Label = a_hc
        Assignment value = 0.7581
        Storage Label = b_hc
        Assignment value = 12.1172
        Storage Label = x0_hc
        Assignment value = 195.7687
        Storage Label = a_LAI
        Assignment value = 3.1487
        Storage Label = b_LAI
        Assignment value = 4.4535
        Storage Label = x0_LAI
        Assignment value = 211.0799
        Storage Label = period_sec
        Assignment value = 3600
Extract
        From Time =
        To Time =
        Channel = 1
        Label for Signal = SECONDS
Extract
        From Time =
        To Time =
        Channel = 2
        Label for Signal = NANOSECONDS
Extract
        From Time =
        To Time =
        Channel = 3
        Label for Signal = RECORD
Extract
        From Time =
        To Time =
        Channel = 4
        Label for Signal = u
Extract
        From Time =
        To Time =
        Channel = 5
        Label for Signal = v
Extract
        From Time =
        To Time =
        Channel = 6
        Label for Signal = w
Extract
        From Time =
        To Time =
        Channel = 7
        Label for Signal = Ts
Extract
        From Time =
        To Time =
        Channel = 8
        Label for Signal = C
Extract
        From Time =
        To Time =
        Channel = 9
        Label for Signal = Q
```

```
Extract
        From Time =
        To Time =
        Channel = 10
        Label for Signal = fw
Extract
        From Time =
        To Time =
        Channel = 11
        Label for Signal = press
Extract
        From Time =
        To Time =
        Channel = 12
        Label for Signal = diag_csat
Extract
        From Time =
        To Time =
        Channel = 13
        Label for Signal = t_hmp
Extract
        From Time =
        To Time =
        Channel = 14
        Label for Signal = e_hmp
User defined
        From Time =
        To Time =
        Storage Label = hc
        Apply to =
        Apply by =
        Equation = a_hc/(1+EXP(-(DAY_OF_YEAR-x0_hc)/b_hc))
        Variable = DAY_OF_YEAR
        Variable = a_hc
        Variable = b_hc
        Variable = x0_hc
User defined
        From Time =
        To Time =
        Storage Label = LAI
        Apply to =
        Apply by =
        Equation = a_LAI/(1+EXP(-(DAY_OF_YEAR-x0_LAI)/b_LAI))
        Variable = DAY_OF_YEAR
        Variable = a_LAI
        Variable = b_LAI
        Variable = x0_LAI
User defined
        From Time =
        To Time =
        Storage Label = d
        Apply to =
        Apply by =
        Equation = hc-hc*((1-EXP(-SQRT(7.5*LAI)))/SQRT(7.5*LAI))
        Variable =  hc
        Variable =  LAI
Mathematical operation
        From Time =
        To Time =
        Storage Label = doh
        Apply to =
        Apply by =
        Measured variable A = d
        Operation  = /
        Measured variable B = hc
Raw Subset
        From Time =
        To Time =
        Subset start time(s) = 0
        Subset length(s) = period_sec
        Signal for condition = diag_csat
        Condition operators = <=
        Condition (lower limit) = 0
        Condition upper limit =
        Storage Label % removed = CSAT_%removed
        Number of signals = 11
        Signal Subset = u
        Signal Subset = v
        Signal Subset = w
        Signal Subset = Ts
        Signal Subset = C
```

```
        Signal Subset = Q
        Signal Subset = fw
        Signal Subset = press
        Signal Subset = diag_csat
        Signal Subset = t_hmp
        Signal Subset = e_hmp
Wind direction
        From Time =
        To Time =
        Signal (u) = u
        Signal (v) = v
        Orientation = 232.433
        Wind Direction Components = U+N_V+W
        Wind Direction Output = N_0_deg-E_90_deg
        Storage Label Wind Direction = wnd_dir
        Storage Label Wind Dir Std Dev = wnd_dir_sd
Rotation coefficients
        From Time =
        To Time =
        Signal (u) = u
        Signal (v) = v
        Signal (w) = w
        Storage Label Alpha =
        Storage Label Beta  =
        Storage Label Gamma =
        Optional mean u =
        Optional mean v =
        Optional mean w =
Rotation
        From Time =
        To Time =
        Signal (u) = u
        Signal (v) = v
        Signal (w) = w
        Alpha =
        Beta =
        Gamma =
        Do 1st Rot = x
        Do 2nd Rot = x
        Do 3rd Rot =
Despike
        From Time =
        To Time =
        Signal = u
        Standard Deviations = 6
        Spike width = 4
        Spike % consistency = 30
        Replace spikes = x
        Storage Label spike count = u_spk
        Outlier Standard Deviations = 6
Despike
        From Time =
        To Time =
        Signal = v
        Standard Deviations = 6
        Spike width = 4
        Spike % consistency = 30
        Replace spikes = x
        Storage Label spike count = v_spk
        Outlier Standard Deviations = 6
Despike
        From Time =
        To Time =
        Signal = w
        Standard Deviations = 6
        Spike width = 4
        Spike % consistency = 30
        Replace spikes = x
        Storage Label spike count = w_spk
        Outlier Standard Deviations = 6
Despike
        From Time =
        To Time =
        Signal = Ts
        Standard Deviations = 6
        Spike width = 4
        Spike % consistency = 30
        Replace spikes = x
        Storage Label spike count = Ts_spk
        Outlier Standard Deviations = 6
Despike
```

```
        From Time =
        To Time =
        Signal = Q
        Standard Deviations = 6
        Spike width = 4
        Spike % consistency = 30
        Replace spikes = x
        Storage Label spike count = Q_spk
        Outlier Standard Deviations = 6
Cross Correlate
        From Time =
        To Time =
        Signal = w
        Signal which lags = Q
        Correlation type = Covariance
        Output Correlation curve =
        Storage Label Peak Time = LagQ
        Storage Label Peak Value =
Remove Lag
        From Time =
        To Time =
        Signal =
        Min Lag (sec) = -0.33
        Lag (sec) = LagQ
        Max Lag (sec) = 0.33
        Below Min default (sec) = 0
        Above Max default (sec) = 0
1 chn statistics
        From Time =
        To Time =
        Signal = u
        Storage Label Mean = u_mean
        Storage Label Std Dev = u_sd
        Storage Label Skewness =
        Storage Label Kurtosis =
        Storage Label Maximum =
        Storage Label Minimum =
        Storage Label Variance =
        Storage Label Turbulent Intensity =
        Alt Turbulent Intensity Denominator =
1 chn statistics
        From Time =
        To Time =
        Signal = v
        Storage Label Mean = v_mean
        Storage Label Std Dev = v_sd
        Storage Label Skewness =
        Storage Label Kurtosis =
        Storage Label Maximum =
        Storage Label Minimum =
        Storage Label Variance =
        Storage Label Turbulent Intensity =
        Alt Turbulent Intensity Denominator =
1 chn statistics
        From Time =
        To Time =
        Signal = w
        Storage Label Mean = w_mean
        Storage Label Std Dev = w_sd
        Storage Label Skewness =
        Storage Label Kurtosis =
        Storage Label Maximum =
        Storage Label Minimum =
        Storage Label Variance =
        Storage Label Turbulent Intensity =
        Alt Turbulent Intensity Denominator =
1 chn statistics
        From Time =
        To Time =
        Signal = Ts
        Storage Label Mean = Ts_mean
        Storage Label Std Dev = Ts_sd
        Storage Label Skewness =
        Storage Label Kurtosis =
        Storage Label Maximum =
        Storage Label Minimum =
        Storage Label Variance =
        Storage Label Turbulent Intensity =
        Alt Turbulent Intensity Denominator =
1 chn statistics
        From Time =
```

```
        To Time =
        Signal = Q
        Storage Label Mean = Q_mean
        Storage Label Std Dev = Q_sd
        Storage Label Skewness =
        Storage Label Kurtosis =
        Storage Label Maximum =
        Storage Label Minimum =
        Storage Label Variance =
        Storage Label Turbulent Intensity =
        Alt Turbulent Intensity Denominator =
1 chn statistics
        From Time =
        To Time =
        Signal = press
        Storage Label Mean = press_mean
        Storage Label Std Dev = press_sd
        Storage Label Skewness =
        Storage Label Kurtosis =
        Storage Label Maximum =
        Storage Label Minimum =
        Storage Label Variance =
        Storage Label Turbulent Intensity =
        Alt Turbulent Intensity Denominator =
1 chn statistics
        From Time =
        To Time =
        Signal = t_hmp
        Storage Label Mean = t_hmp_mean
        Storage Label Std Dev = t_hmp_sd
        Storage Label Skewness =
        Storage Label Kurtosis =
        Storage Label Maximum =
        Storage Label Minimum =
        Storage Label Variance =
        Storage Label Turbulent Intensity =
        Alt Turbulent Intensity Denominator =
1 chn statistics
        From Time =
        To Time =
        Signal = e_hmp
        Storage Label Mean = e_hmp_mean
        Storage Label Std Dev = e_hmp_sd
        Storage Label Skewness =
        Storage Label Kurtosis =
        Storage Label Maximum =
        Storage Label Minimum =
        Storage Label Variance =
        Storage Label Turbulent Intensity =
        Alt Turbulent Intensity Denominator =
Gas conversion time series
        From Time =
        To Time =
        Signal = Q
        Convert from = Absolute density g/m3
        Convert to = Molar density mmol/m3
        1st Offset = 0
        1st Gain = 1
        1st Curvature = 0
        Signal T, C =
        Value T, C =
        Signal P, kPa =
        Value P, kPa =
        Signal H2O =
        Value H2O =
        Units H2O =
        Molecular Weight = 18.015
        2nd Offset = 0
        2nd Gain = 1
        2nd Curvature = 0
Virtual Temperature Raw
        From Time =
        To Time =
        Signal T(C) =  Ts
        Signal H2O =   Q
        Pressure, kPa =  press_mean
        Water vapour units =  Molar density, mmol/m3
        Temperature conversion = Calculate true from virtual-sonic
1 chn statistics
        From Time =
        To Time =
```

```
        Signal = Ts
        Storage Label Mean = T_mean
        Storage Label Std Dev = T_sd
        Storage Label Skewness =
        Storage Label Kurtosis =
        Storage Label Maximum =
        Storage Label Minimum =
        Storage Label Variance =
        Storage Label Turbulent Intensity =
        Alt Turbulent Intensity Denominator =
Gas conversion time series
        From Time =
        To Time =
        Signal = Q
        Convert from = Molar density mmol/m3
        Convert to = Absolute density g/m3
        1st Offset = 0
        1st Gain = 1
        1st Curvature = 0
        Signal T, C =
        Value T, C =
        Signal P, kPa =
        Value P, kPa =
        Signal H2O =
        Value H2O =
        Units H2O =
        Molecular Weight = 18.015
        2nd Offset = 0
        2nd Gain = 1
        2nd Curvature = 0
Partial pressure
        From Time =
        To Time =
        Storage Label = e
        Apply to =
        Apply by =
        Variable type = Absolute density
        Measured variable = Q_mean
        Min or QC =
        Max or QC =
        Temperature (C) = T_mean
        Min or QC =
        Max or QC =
        Pressure (KPa) = press_kPa
        Min or QC =
        Max or QC =
        Molecular weight (g/mole) = 18.015
        Conc conv factor = 1000
Latent heat of evaporation
        From Time =
        To Time =
        Storage Label = LV
        Apply to =
        Apply by =
        Temperature (C) = T_mean
        Min or QC =
        Max or QC =
        Pressure (KPa) = press_mean
        Min or QC =
        Max or QC =
        LE flux coef, L = 2450
Sensible heat flux coefficient
        From Time =
        To Time =
        Storage Label = rhoCp
        Apply to =
        Apply by =
        Vapour pressure (KPa) = e
        Min or QC =
        Max or QC =
        Temperature (C) = T_mean
        Min or QC =
        Max or QC =
        Pressure (KPa) = press_mean
        Min or QC =
        Max or QC =
        Alternate rhoCp = 1296.0243
2 chn statistics
        From Time =
        To Time =
        Signal = w
```

```
        Signal = Q
        Storage Label Covariance = cov_wQ
        Storage Label Correlation =
        Storage Label Flux = LE'
        Flux coefficient = LV
2 chn statistics
        From Time =
        To Time =
        Signal = w
        Signal = Ts
        Storage Label Covariance = cov_wTs
        Storage Label Correlation =
        Storage Label Flux = Hs'
        Flux coefficient = rhoCp
2 chn statistics
        From Time =
        To Time =
        Signal = w
        Signal = v
        Storage Label Covariance = cov_vw'
        Storage Label Correlation =
        Storage Label Flux =
        Flux coefficient =
2 chn statistics
        From Time =
        To Time =
        Signal = w
        Signal = u
        Storage Label Covariance = cov_uw'
        Storage Label Correlation =
        Storage Label Flux =
        Flux coefficient =
Friction Velocity
        From Time =
        To Time =
        Signal (u) = u
        Signal (v) = v
        Signal (w) = w
        Storage Label U* (uw) =
        Storage Label U* (uw vw) = ustar
Comments
        Comment = Start of iteration
        Comment =
        Comment =
User defined
        From Time =
        To Time =
        Storage Label = ustar_iter
        Apply to =
        Apply by =
        Equation = (cov_uw^2+cov_vw^2)^0.25
        Variable = cov_uw
        Variable = cov_vw
Stability - Monin Obhukov
        From Time =
        To Time =
        Storage Label = ZoL
        Apply to =
        Apply by =
        Measurement height (m) = z
        Zero plane displacement (m) = d
        Virtual Temperature (C) = Ts_mean
        Min or QC =
        Max or QC =
        H flux (W/m2) = Hs'
        Min or QC =
        Max or QC =
        H flux coef, RhoCp = rhoCp
        Min or QC =
        Max or QC =
        Scaling velocity (m/s) = ustar_iter
        Min or QC =
        Max or QC =
Frequency response
        From Time =
        To Time =
        Storage Label = UW_fr_M86
        Apply to =
        Apply by =
        Correction type = UW
        Measurement height (m) = z
```

```
        Zero plane displacement (m) = d
        Boundary layer height (m) = 900
        Stability Z/L = ZoL
        Wind speed (m/s) = u_mean
        Sensor 1 Flow velocity (m/s) = u_mean
        Sensor 1 Sampling frequency (Hz) = 20
        Sensor 1 Low pass filter type =
        Sensor 1 Low pass filter time constant =
        Sensor 1 High pass filter type =
        Sensor 1 High pass filter time constant =
        Sensor 1 Path length (m) = CSATSclrPL
        Sensor 1 Time constant (s) = 0
        Sensor 1 Tube attenuation coef =
        Sensor 2 Flow velocity (m/s) = u_mean
        Sensor 2 Sampling frequency (Hz) = 20
        Sensor 2 Low pass filter type =
        Sensor 2 Low pass filter time constant =
        Sensor 2 High pass filter type =
        Sensor 2 High pass filter time constant =
        Sensor 2 Path length (m) = CSATSclrPL
        Sensor 2 Time constant (s) = 0
        Sensor 2 Tube attenuation coef =
        Path separation (m) = 0
        Get spectral data type =  Model
        Get response function from = model
        Reference Tag =
        Reference response condition =
        Sensor 1 subsampled =
        Sensor 2 subsampled =
        Apply velocity distribution adjustment =
        Use calculated distribution =
        Velocity distribution std dev=
        Stability distribution std dev=
Frequency response
        From Time =
        To Time =
        Storage Label = H_fr_M86
        Apply to =
        Apply by =
        Correction type = WX
        Measurement height (m) = z
        Zero plane displacement (m) = d
        Boundary layer height (m) = 900
        Stability Z/L = ZoL
        Wind speed (m/s) = u_mean
        Sensor 1 Flow velocity (m/s) = u_mean
        Sensor 1 Sampling frequency (Hz) = 20
        Sensor 1 Low pass filter type =
        Sensor 1 Low pass filter time constant =
        Sensor 1 High pass filter type =
        Sensor 1 High pass filter time constant =
        Sensor 1 Path length (m) = CSATSclrPL
        Sensor 1 Time constant (s) = 0
        Sensor 1 Tube attenuation coef =
        Sensor 2 Flow velocity (m/s) = u_mean
        Sensor 2 Sampling frequency (Hz) = 20
        Sensor 2 Low pass filter type =
        Sensor 2 Low pass filter time constant =
        Sensor 2 High pass filter type =
        Sensor 2 High pass filter time constant =
        Sensor 2 Path length (m) = CSATSclrPL
        Sensor 2 Time constant (s) = 0
        Sensor 2 Tube attenuation coef =
        Path separation (m) = 0
        Get spectral data type = Model
        Get response function from = model
        Reference Tag =
        Reference response condition =
        Sensor 1 subsampled =
        Sensor 2 subsampled =
        Apply velocity distribution adjustment =
        Use calculated distribution =
        Velocity distribution std dev=
        Stability distribution std dev=
Frequency response
        From Time =
        To Time =
        Storage Label = LE_fr_M86
        Apply to =
        Apply by =
        Correction type = WX
```

```
        Measurement height (m) = z
        Zero plane displacement (m) = d
        Boundary layer height (m) = 900
        Stability Z/L = ZoL
        Wind speed (m/s) = u_mean
        Sensor 1 Flow velocity (m/s) = u_mean
        Sensor 1 Sampling frequency (Hz) = 20
        Sensor 1 Low pass filter type =
        Sensor 1 Low pass filter time constant =
        Sensor 1 High pass filter type =
        Sensor 1 High pass filter time constant =
        Sensor 1 Path length (m) = CSATSclrPL
        Sensor 1 Time constant (s) = 0
        Sensor 1 Tube attenuation coef =
        Sensor 2 Flow velocity (m/s) = u_mean
        Sensor 2 Sampling frequency (Hz) = 20
        Sensor 2 Low pass filter type =
        Sensor 2 Low pass filter time constant =
        Sensor 2 High pass filter type =
        Sensor 2 High pass filter time constant =
        Sensor 2 Path length (m) = LiCor7500PL
        Sensor 2 Time constant (s) = 0
        Sensor 2 Tube attenuation coef =
        Path separation (m) = 0.1
        Get spectral data type = Model
        Get response function from = model
        Reference Tag =
        Reference response condition =
        Sensor 1 subsampled =
        Sensor 2 subsampled =
        Apply velocity distribution adjustment =
        Use calculated distribution =
        Velocity distribution std dev=
        Stability distribution std dev=
Mathematical operation
        From Time =
        To Time =
        Storage Label = cov_uw
        Apply to =
        Apply by =
        Measured variable A = cov_uw'
        Operation  = *
        Measured variable B = UW_fr_M86
Mathematical operation
        From Time =
        To Time =
        Storage Label = cov_vw
        Apply to =
        Apply by =
        Measured variable A = cov_vw'
        Operation  = *
        Measured variable B = UW_fr_M86
Mathematical operation
        From Time =
        To Time =
        Storage Label = Hs
        Apply to =
        Apply by =
        Measured variable A = Hs'
        Operation  = *
        Measured variable B = H_fr_M86
Mathematical operation
        From Time =
        To Time =
        Storage Label = LE
        Apply to =
        Apply by =
        Measured variable A = LE'
        Operation  = *
        Measured variable B = LE_fr_M86
Sonic T - heat flux correction
        From Time =
        To Time =
        Storage Label = HFC
        Apply to =  Hs
        Apply by =  +
        Temperatue (C) = T_mean
        Min or QC =
        Max or QC =
        Wind speed (m/s) = 0
        Min or QC =
```

```
        Max or QC =
        Vapour pressure (KPa)  = e
        Min or QC =
        Max or QC =
        Pressure (KPa) = press_mean
        Min or QC =
        Max or QC =
        uw covariance (m2/s2) = 0
        Min or QC =
        Max or QC =
        LE flux (W/m2) = LE
        Min or QC =
        Max or QC =
        LE flux coef, L = LV
        Min or QC =
        Max or QC =
        H flux coef, RhoCp = rhoCp
        Min or QC =
        Max or QC =
        Temperature (C) Alt  =
        Wind speed (m/s) Alt  =
        Vapour pressure (KPa) Alt =
        Pressure (KPa) Alt =
Webb correction
        From Time =
        To Time =
        Storage Label = WPL
        Apply to = LE
        Apply by = +
        Scalar value type = Density (g/m3)
        Scalar value = Q_mean
        Min or QC =
        Max or QC =
        Water vapour value type = Density (g/m3)
        Water vapour value = Q_mean
        Min or QC =
        Max or QC =
        Temperature (C) = T_mean
        Min or QC =
        Max or QC =
        Pressure (KPa) = press_mean
        Min or QC =
        Max or QC =
        H flux (W/m2) = Hs
        Min or QC =
        Max or QC =
        LE flux (W/m2) = LE
        Min or QC =
        Max or QC =
        H flux coef, RhoCp = rhoCp
        Min or QC =
        Max or QC =
        LE flux coef, L = LV
        Min or QC =
        Max or QC =
        Scalar molecular wt. = 18.015
        Scalar flux type = LE (W/m2)
        Scalar flux coefficient =
        Min or QC =
        Max or QC =
        Alternate water vapour pressure (kPa) =
        Alternate temperature (C) =
        Alternate pressure (kPa) =
User defined
        From Time =
        To Time =
        Storage Label = ustar_iter
        Apply to =
        Apply by =
        Equation = (cov_uw^2+cov_vw^2)^0.25
        Variable = cov_uw
        Variable = cov_vw
Stability - Monin Obhukov
        From Time =
        To Time =
        Storage Label = ZoL
        Apply to =
        Apply by =
        Measurement height (m) = z
        Zero plane displacement (m) = d
        Virtual Temperature (C) = Ts_mean
```

```
        Min or QC =
        Max or QC =
        H flux (W/m2) = Hs
        Min or QC =
        Max or QC =
        H flux coef, RhoCp = rhoCp
        Min or QC =
        Max or QC =
        Scaling velocity (m/s) = ustar_iter
        Min or QC =
        Max or QC =
Frequency response
        From Time =
        To Time =
        Storage Label = UW_fr_M86
        Apply to =
        Apply by =
        Correction type = UW
        Measurement height (m) = z
        Zero plane displacement (m) = d
        Boundary layer height (m) = 900
        Stability Z/L = ZoL
        Wind speed (m/s) = u_mean
        Sensor 1 Flow velocity (m/s) = u_mean
        Sensor 1 Sampling frequency (Hz) = 20
        Sensor 1 Low pass filter type =
        Sensor 1 Low pass filter time constant =
        Sensor 1 High pass filter type =
        Sensor 1 High pass filter time constant =
        Sensor 1 Path length (m) = CSATSclrPL
        Sensor 1 Time constant (s) = 0
        Sensor 1 Tube attenuation coef =
        Sensor 2 Flow velocity (m/s) = u_mean
        Sensor 2 Sampling frequency (Hz) = 20
        Sensor 2 Low pass filter type =
        Sensor 2 Low pass filter time constant =
        Sensor 2 High pass filter type =
        Sensor 2 High pass filter time constant =
        Sensor 2 Path length (m) = CSATSclrPL
        Sensor 2 Time constant (s) = 0
        Sensor 2 Tube attenuation coef =
        Path separation (m) = 0
        Get spectral data type =  Model
        Get response function from = model
        Reference Tag =
        Reference response condition =
        Sensor 1 subsampled =
        Sensor 2 subsampled =
        Apply velocity distribution adjustment =
        Use calculated distribution =
        Velocity distribution std dev=
        Stability distribution std dev=
Frequency response
        From Time =
        To Time =
        Storage Label = H_fr_M86
        Apply to =
        Apply by =
        Correction type = WX
        Measurement height (m) = z
        Zero plane displacement (m) = d
        Boundary layer height (m) = 900
        Stability Z/L = ZoL
        Wind speed (m/s) = u_mean
        Sensor 1 Flow velocity (m/s) = u_mean
        Sensor 1 Sampling frequency (Hz) = 20
        Sensor 1 Low pass filter type =
        Sensor 1 Low pass filter time constant =
        Sensor 1 High pass filter type =
        Sensor 1 High pass filter time constant =
        Sensor 1 Path length (m) = CSATSclrPL
        Sensor 1 Time constant (s) = 0
        Sensor 1 Tube attenuation coef =
        Sensor 2 Flow velocity (m/s) = u_mean
        Sensor 2 Sampling frequency (Hz) = 20
        Sensor 2 Low pass filter type =
        Sensor 2 Low pass filter time constant =
        Sensor 2 High pass filter type =
        Sensor 2 High pass filter time constant =
        Sensor 2 Path length (m) = CSATSclrPL
        Sensor 2 Time constant (s) = 0
```

```
        Sensor 2 Tube attenuation coef =
        Path separation (m) = 0
        Get spectral data type = Model
        Get response function from = model
        Reference Tag =
        Reference response condition =
        Sensor 1 subsampled =
        Sensor 2 subsampled =
        Apply velocity distribution adjustment =
        Use calculated distribution =
        Velocity distribution std dev=
        Stability distribution std dev=
Frequency response
        From Time =
        To Time =
        Storage Label = LE_fr_M86
        Apply to =
        Apply by =
        Correction type = WX
        Measurement height (m) = z
        Zero plane displacement (m) = d
        Boundary layer height (m) = 900
        Stability Z/L = ZoL
        Wind speed (m/s) = u_mean
        Sensor 1 Flow velocity (m/s) = u_mean
        Sensor 1 Sampling frequency (Hz) = 20
        Sensor 1 Low pass filter type =
        Sensor 1 Low pass filter time constant =
        Sensor 1 High pass filter type =
        Sensor 1 High pass filter time constant =
        Sensor 1 Path length (m) = CSATSclrPL
        Sensor 1 Time constant (s) = 0
        Sensor 1 Tube attenuation coef =
        Sensor 2 Flow velocity (m/s) = u_mean
        Sensor 2 Sampling frequency (Hz) = 20
        Sensor 2 Low pass filter type =
        Sensor 2 Low pass filter time constant =
        Sensor 2 High pass filter type =
        Sensor 2 High pass filter time constant =
        Sensor 2 Path length (m) = LiCor7500PL
        Sensor 2 Time constant (s) = 0
        Sensor 2 Tube attenuation coef =
        Path separation (m) = 0.1
        Get spectral data type = Model
        Get response function from = model
        Reference Tag =
        Reference response condition =
        Sensor 1 subsampled =
        Sensor 2 subsampled =
        Apply velocity distribution adjustment =
        Use calculated distribution =
        Velocity distribution std dev=
        Stability distribution std dev=
Mathematical operation
        From Time =
        To Time =
        Storage Label = cov_uw
        Apply to =
        Apply by =
        Measured variable A = cov_uw'
        Operation  = *
        Measured variable B = UW_fr_M86
Mathematical operation
        From Time =
        To Time =
        Storage Label = cov_vw
        Apply to =
        Apply by =
        Measured variable A = cov_vw'
        Operation  = *
        Measured variable B = UW_fr_M86
Mathematical operation
        From Time =
        To Time =
        Storage Label = Hs
        Apply to =
        Apply by =
        Measured variable A = Hs'
        Operation  = *
        Measured variable B = H_fr_M86
Mathematical operation
```

```
        From Time =
        To Time =
        Storage Label = LE
        Apply to =
        Apply by =
        Measured variable A = LE'
        Operation  = *
        Measured variable B = LE_fr_M86
Sonic T - heat flux correction
        From Time =
        To Time =
        Storage Label = HFC
        Apply to = Hs
        Apply by = +
        Temperatue (C) = T_mean
        Min or QC =
        Max or QC =
        Wind speed (m/s) = 0
        Min or QC =
        Max or QC =
        Vapour pressure (KPa)  = e
        Min or QC =
        Max or QC =
        Pressure (KPa) = press_mean
        Min or QC =
        Max or QC =
        uw covariance (m2/s2) = 0
        Min or QC =
        Max or QC =
        LE flux (W/m2) = LE
        Min or QC =
        Max or QC =
        LE flux coef, L = LV
        Min or QC =
        Max or QC =
        H flux coef, RhoCp = rhoCp
        Min or QC =
        Max or QC =
        Temperature (C) Alt  =
        Wind speed (m/s) Alt  =
        Vapour pressure (KPa) Alt =
        Pressure (KPa) Alt =
Webb correction
        From Time =
        To Time =
        Storage Label = WPL
        Apply to = LE
        Apply by = +
        Scalar value type = Density (g/m3)
        Scalar value = Q_mean
        Min or QC =
        Max or QC =
        Water vapour value type = Density (g/m3)
        Water vapour value = Q_mean
        Min or QC =
        Max or QC =
        Temperature (C) = T_mean
        Min or QC =
        Max or QC =
        Pressure (KPa) = press_mean
        Min or QC =
        Max or QC =
        H flux (W/m2) = Hs
        Min or QC =
        Max or QC =
        LE flux (W/m2) = LE
        Min or QC =
        Max or QC =
        H flux coef, RhoCp = rhoCp
        Min or QC =
        Max or QC =
        LE flux coef, L = LV
        Min or QC =
        Max or QC =
        Scalar molecular wt. = 18.015
        Scalar flux type = LE (W/m2)
        Scalar flux coefficient =
        Min or QC =
        Max or QC =
        Alternate water vapour pressure (kPa) =
        Alternate temperature (C) =
```

```
        Alternate pressure (kPa) =
User defined
        From Time =
        To Time =
        Storage Label = ustar_iter
        Apply to =
        Apply by =
        Equation = (cov_uw^2+cov_vw^2)^0.25
        Variable = cov_uw
        Variable = cov_vw
Stability - Monin Obhukov
        From Time =
        To Time =
        Storage Label = ZoL
        Apply to =
        Apply by =
        Measurement height (m) = z
        Zero plane displacement (m) = d
        Virtual Temperature (C) = Ts_mean
        Min or QC =
        Max or QC =
        H flux (W/m2) = Hs
        Min or QC =
        Max or QC =
        H flux coef, RhoCp = rhoCp
        Min or QC =
        Max or QC =
        Scaling velocity (m/s) = ustar_iter
        Min or QC =
        Max or QC =
Frequency response
        From Time =
        To Time =
        Storage Label = UW_fr_M86
        Apply to =
        Apply by =
        Correction type = UW
        Measurement height (m) = z
        Zero plane displacement (m) = d
        Boundary layer height (m) = 900
        Stability Z/L = ZoL
        Wind speed (m/s) = u_mean
        Sensor 1 Flow velocity (m/s) = u_mean
        Sensor 1 Sampling frequency (Hz) = 20
        Sensor 1 Low pass filter type =
        Sensor 1 Low pass filter time constant =
        Sensor 1 High pass filter type =
        Sensor 1 High pass filter time constant =
        Sensor 1 Path length (m) = CSATSclrPL
        Sensor 1 Time constant (s) = 0
        Sensor 1 Tube attenuation coef =
        Sensor 2 Flow velocity (m/s) = u_mean
        Sensor 2 Sampling frequency (Hz) = 20
        Sensor 2 Low pass filter type =
        Sensor 2 Low pass filter time constant =
        Sensor 2 High pass filter type =
        Sensor 2 High pass filter time constant =
        Sensor 2 Path length (m) = CSATSclrPL
        Sensor 2 Time constant (s) = 0
        Sensor 2 Tube attenuation coef =
        Path separation (m) = 0
        Get spectral data type =  Model
        Get response function from = model
        Reference Tag =
        Reference response condition =
        Sensor 1 subsampled =
        Sensor 2 subsampled =
        Apply velocity distribution adjustment =
        Use calculated distribution =
        Velocity distribution std dev=
        Stability distribution std dev=
Frequency response
        From Time =
        To Time =
        Storage Label = H_fr_M86
        Apply to =
        Apply by =
        Correction type = WX
        Measurement height (m) = z
        Zero plane displacement (m) = d
        Boundary layer height (m) = 900
```

```
        Stability Z/L = ZoL
        Wind speed (m/s) = u_mean
        Sensor 1 Flow velocity (m/s) = u_mean
        Sensor 1 Sampling frequency (Hz) = 20
        Sensor 1 Low pass filter type =
        Sensor 1 Low pass filter time constant =
        Sensor 1 High pass filter type =
        Sensor 1 High pass filter time constant =
        Sensor 1 Path length (m) = CSATSclrPL
        Sensor 1 Time constant (s) = 0
        Sensor 1 Tube attenuation coef =
        Sensor 2 Flow velocity (m/s) = u_mean
        Sensor 2 Sampling frequency (Hz) = 20
        Sensor 2 Low pass filter type =
        Sensor 2 Low pass filter time constant =
        Sensor 2 High pass filter type =
        Sensor 2 High pass filter time constant =
        Sensor 2 Path length (m) = CSATSclrPL
        Sensor 2 Time constant (s) = 0
        Sensor 2 Tube attenuation coef =
        Path separation (m) = 0
        Get spectral data type = Model
        Get response function from = model
        Reference Tag =
        Reference response condition =
        Sensor 1 subsampled =
        Sensor 2 subsampled =
        Apply velocity distribution adjustment =
        Use calculated distribution =
        Velocity distribution std dev=
        Stability distribution std dev=
Frequency response
        From Time =
        To Time =
        Storage Label = LE_fr_M86
        Apply to =
        Apply by =
        Correction type = WX
        Measurement height (m) = z
        Zero plane displacement (m) = d
        Boundary layer height (m) = 900
        Stability Z/L = ZoL
        Wind speed (m/s) = u_mean
        Sensor 1 Flow velocity (m/s) = u_mean
        Sensor 1 Sampling frequency (Hz) = 20
        Sensor 1 Low pass filter type =
        Sensor 1 Low pass filter time constant =
        Sensor 1 High pass filter type =
        Sensor 1 High pass filter time constant =
        Sensor 1 Path length (m) = CSATSclrPL
        Sensor 1 Time constant (s) = 0
        Sensor 1 Tube attenuation coef =
        Sensor 2 Flow velocity (m/s) = u_mean
        Sensor 2 Sampling frequency (Hz) = 20
        Sensor 2 Low pass filter type =
        Sensor 2 Low pass filter time constant =
        Sensor 2 High pass filter type =
        Sensor 2 High pass filter time constant =
        Sensor 2 Path length (m) = LiCor7500PL
        Sensor 2 Time constant (s) = 0
        Sensor 2 Tube attenuation coef =
        Path separation (m) = 0.1
        Get spectral data type = Model
        Get response function from = model
        Reference Tag =
        Reference response condition =
        Sensor 1 subsampled =
        Sensor 2 subsampled =
        Apply velocity distribution adjustment =
        Use calculated distribution =
        Velocity distribution std dev=
        Stability distribution std dev=
Mathematical operation
        From Time =
        To Time =
        Storage Label = cov_uw
        Apply to =
        Apply by =
        Measured variable A = cov_uw'
        Operation  = *
        Measured variable B = UW_fr_M86
```

```
Mathematical operation
        From Time =
        To Time =
        Storage Label = cov_vw
        Apply to =
        Apply by =
        Measured variable A = cov_vw'
        Operation  = *
        Measured variable B = UW_fr_M86
Mathematical operation
        From Time =
        To Time =
        Storage Label = Hs
        Apply to =
        Apply by =
        Measured variable A = Hs'
        Operation  = *
        Measured variable B = H_fr_M86
Mathematical operation
        From Time =
        To Time =
        Storage Label = LE
        Apply to =
        Apply by =
        Measured variable A = LE'
        Operation  = *
        Measured variable B = LE_fr_M86
Sonic T - heat flux correction
        From Time =
        To Time =
        Storage Label = HFC
        Apply to = Hs
        Apply by = +
        Temperatue (C) = T_mean
        Min or QC =
        Max or QC =
        Wind speed (m/s) = 0
        Min or QC =
        Max or QC =
        Vapour pressure (KPa)  = e
        Min or QC =
        Max or QC =
        Pressure (KPa) = press_mean
        Min or QC =
        Max or QC =
        uw covariance (m2/s2) = 0
        Min or QC =
        Max or QC =
        LE flux (W/m2) = LE
        Min or QC =
        Max or QC =
        LE flux coef, L = LV
        Min or QC =
        Max or QC =
        H flux coef, RhoCp = rhoCp
        Min or QC =
        Max or QC =
        Temperature (C) Alt  =
        Wind speed (m/s) Alt  =
        Vapour pressure (KPa) Alt =
        Pressure (KPa) Alt =
Webb correction
        From Time =
        To Time =
        Storage Label = WPL
        Apply to = LE
        Apply by = +
        Scalar value type = Density (g/m3)
        Scalar value = Q_mean
        Min or QC =
        Max or QC =
        Water vapour value type = Density (g/m3)
        Water vapour value = Q_mean
        Min or QC =
        Max or QC =
        Temperature (C) = T_mean
        Min or QC =
        Max or QC =
        Pressure (KPa) = press_mean
        Min or QC =
        Max or QC =
```

```
        H flux (W/m2) = Hs
        Min or QC =
        Max or QC =
        LE flux (W/m2) = LE
        Min or QC =
        Max or QC =
        H flux coef, RhoCp = rhoCp
        Min or QC =
        Max or QC =
        LE flux coef, L = LV
        Min or QC =
        Max or QC =
        Scalar molecular wt. = 18.015
        Scalar flux type = LE (W/m2)
        Scalar flux coefficient =
        Min or QC =
        Max or QC =
        Alternate water vapour pressure (kPa) =
        Alternate temperature (C) =
        Alternate pressure (kPa) =
Comments
        Comment = End of iteration
        Comment =
        Comment =
User defined
        From Time =
        To Time =
        Storage Label = rho_w
        Apply to =
        Apply by =
        Equation = 999.168-(0.1474*T_mean)-(0.0064844*(T_mean^2))+(0.000050868*(T_mean^3))
        Variable = T_mean
User defined
        From Time =
        To Time =
        Storage Label = ET_mmh^-1
        Apply to =
        Apply by =
        Equation = (LE*3.6)/((LV/1000)*rho_w)
        Variable = LE
        Variable = rho_w
        Variable = LV
Mathematical operation
        From Time =
        To Time =
        Storage Label = H+LE
        Apply to =
        Apply by =
        Measured variable A = LE
        Operation  = +
        Measured variable B = Hs
Mathematical operation
        From Time =
        To Time =
        Storage Label = BR
        Apply to =
        Apply by =
        Measured variable A = Hs
        Operation  = /
        Measured variable B = LE
Roughness length (zo)
        From Time =
        To Time =
        Storage Label = Zo
        Apply to =
        Apply by =
        Scaling velocity (m/s) = ustar_iter
        Min or QC =
        Max or QC =
        Wind speed (m/s) = u_mean
        Min or QC =
        Max or QC =
        Measurement height (m) = z
        Zero plane displacement (m) = d
User defined
        From Time =
        To Time =
        Storage Label = L
        Apply to =
        Apply by =
        Equation = (z-d)/ZoL
```

```
        Variable = z
        Variable = d
        Variable = ZoL
Stationarity
        From Time =
        To Time =
        Signal (A) = u
        Signal (B) = w
        Storage Label A StdDev Stationarity =
        Storage Label B StdDev Stationarity =
        Storage Label AB Covariance Stationarity = uw_station
        Segment length, minutes = 5
        Linear detrend segments =
        Linear detrend run =
        Storage Label AB StdDev Stationarity =
Stationarity
        From Time =
        To Time =
        Signal (A) = Ts
        Signal (B) = w
        Storage Label A StdDev Stationarity =
        Storage Label B StdDev Stationarity =
        Storage Label AB Covariance Stationarity = wTs_station
        Segment length, minutes = 5
        Linear detrend segments =
        Linear detrend run =
        Storage Label AB StdDev Stationarity =
Stationarity
        From Time =
        To Time =
        Signal (A) = Q
        Signal (B) = w
        Storage Label A StdDev Stationarity =
        Storage Label B StdDev Stationarity =
        Storage Label AB Covariance Stationarity = wQ_station
        Segment length, minutes = 5
        Linear detrend segments =
        Linear detrend run =
        Storage Label AB StdDev Stationarity =
Integral Turbulence
        From Time =
        To Time =
        Signal = u
        Signal(w) = w
        Storage Label QC value = ITTu
        Type of signal = U
        Friction velocity (U*) = ustar_iter
        Monin Ohbukov stability = ZoL
        Latitude, deg = 35.1883
        Alternate turbulent intensity model value =
Integral Turbulence
        From Time =
        To Time =
        Signal = w
        Signal(w) = w
        Storage Label QC value = ITTw
        Type of signal = W
        Friction velocity (U*) = ustar_iter
        Monin Ohbukov stability = ZoL
        Latitude, deg = 35.1883
        Alternate turbulent intensity model value =
Integral Turbulence
        From Time =
        To Time =
        Signal = Ts
        Signal(w) = w
        Storage Label QC value = ITTt
        Type of signal = X
        Friction velocity (U*) = ustar_iter
        Monin Ohbukov stability = ZoL
        Latitude, deg = 35.1883
        Alternate turbulent intensity model value =
User defined
        From Time =
        To Time =
        Storage Label = zu
        Apply to =
        Apply by =
        Equation = (z-d)*(LN((z-d)/Zo)-1+(Zo/(z-d)))
        Variable = z
        Variable = d
```

```
        Variable = Zo
User defined
        From Time =
        To Time =
        Storage Label = zm
        Apply to =
        Apply by =
        Equation = z-d
        Variable = z
        Variable = d
```

APPENDIX B: MATLAB CODE FOR S90 AND H2000 FOOTPRINT MODELS

```
clear
clc
%Import data from Excel spreadsheet
temp=xlsread('S&H_input.xlsx');
S=temp(:,1);
H=temp(:,2);
D=temp(:,3);
E=temp(:,4);
theta=temp(:,5);
xprime=xlsread('xprime.xlsx');
yprime=xlsread('yprime.xlsx');
NE=xlsread('NE.xlsx');
SE=xlsread('SE.xlsx');
SW=xlsread('SW.xlsx');
NW=xlsread('NW.xlsx');
output=NaN(size(theta,1),10);
for i=1:size(theta,1)
   %Rotate coordinates into mean wind direction
   if (theta(i)>(-360)) && (theta(i)<360)
      X=-yprime*sin(theta(i)*pi/180)+xprime*cos(theta(i)*pi/180);
      Y=yprime*cos(theta(i)*pi/180)+xprime*sin(theta(i)*pi/180);
      %Calculate the footprint functions
      for m=1:size(xprime,1)
         for n=1:size(xprime,2)
            if X(m,n)>0
               F_S(m,n)=(S(i)/(X(m,n)^2))*exp(-S(i)/X(m,n))*exp(-
                      (Y(m,n)^2)/(2*(D(i)*X(m,n)^E(i))^2))/
                       (sqrt(2*pi)*D(i)*X(m,n)^E(i));
               F_H(m,n)=(H(i)/(X(m,n)^2))*exp(-H(i)/X(m,n))*exp(-
                      (Y(m,n)^2)/(2*(D(i)*X(m,n)^E(i))^2))/
                       (sqrt(2*pi)*D(i)*X(m,n)^E(i));
            else
               F_S(m,n)=0;
               F_H(m,n)=0;
            end
         end
      end
      %Calculate the cumulative footprint weight for each field
      output(i,1)=sum(sum(F_S));
      FNE_S=F_S.*NE;
      output(i,2)=sum(sum(FNE_S));
      FSE_S=F_S.*SE;
      output(i,3)=sum(sum(FSE_S));
      FSW_S=F_S.*SW;
      output(i,4)=sum(sum(FSW_S));
      FNW_S=F_S.*NW;
      output(i,5)=sum(sum(FNW_S));
      output(i,6)=sum(sum(F_H));
      FNE_H=F_H.*NE;
      output(i,7)=sum(sum(FNE_H));
      FSE_H=F_H.*SE;
      output(i,8)=sum(sum(FSE_H));
      FSW_H=F_H.*SW;
      output(i,9)=sum(sum(FSW_H));
      FNW_H=F_H.*NW;
      output(i,10)=sum(sum(FNW_H));

   end
end
```

APPENDIX C: MATLAB CODE FOR KM01 FOOTPRINT MODEL

```
clear
clc
%Import data from Excel spreadsheet
temp=xlsread('KM_input_1NE.xlsx');
A=temp(:,1);
B=temp(:,2);
C=temp(:,3);
D=temp(:,4);
E=temp(:,5);
theta=temp(:,6);
xprime=xlsread('xprime1.xlsx');
yprime=xlsread('yprime1.xlsx');
NE=xlsread('NE.xlsx');
SE=xlsread('SE.xlsx');
SW=xlsread('SW.xlsx');
NW=xlsread('NW.xlsx');
output=NaN(size(theta,1),5);
for i=1:size(theta,1)
   %Rotate coordinates into mean wind direction
   if (theta(i)>(-360)) && (theta(i)<360)
      X=-yprime*sin(theta(i)*pi/180)+xprime*cos(theta(i)*pi/180);
      Y=yprime*cos(theta(i)*pi/180)+xprime*sin(theta(i)*pi/180);
      %Calculate the footprint weights
      for m=1:size(xprime,1)
          for n=1:size(xprime,2)
              if X(m,n)>0
                  F(m,n)=(1/(sqrt(2*pi)*D(i)*X(m,n)^E(i)))*exp(
                          -(Y(m,n)^2/(2*(D(i)*X(m,n)^E(i))^2)))
                          *C(i)*X(m,n)^-A(i)*exp(-B(i)/X(m,n));
              else
                  F(m,n)=0;
              end
          end
      end
      output(i,1)=sum(sum(F));
      %Calculate cumulative footprint weight for each field
      FNE=F.*NE;
      output(i,2)=sum(sum(FNE));
      FSE=F.*SE;
      output(i,3)=sum(sum(FSE));
      FSW=F.*SW;
      output(i,4)=sum(sum(FSW));
      FNW=F.*NW;
      output(i,5)=sum(sum(FNW));
   end
end
```

APPENDIX D: DAILY ET

Table D.1: Daily ET from NE and SE lysimeters, grass reference ET, and precipitation for each DOY during the study period.

	NE Lysimeter		SE Lysimeter			
	ET	Notes	ET	Notes	ETg	Precip
DOY	mm		mm		mm	mm
158	2.7		3.0			0.0
159	1.8		1.8		9.4	0.0
160	-4.0		-4.0		6.5	5.8
161	3.9		3.8		5.5	0.1
162	1.7		1.8		8.6	0.0
163	2.8		2.3		11.4	0.0
164	1.3		1.2		7.2	0.0
165	1.2		0.9		6.9	0.0
166	0.9		1.1		6.9	0.0
167	2.0		1.6		8.2	0.0
168	-15.3		-15.0		7.2	17.6
169	-4.2		-2.6		3.8	5.3
170	2.8		2.8		6.3	2.7
171	-0.3		-0.8	F	5.1	3.2
172	-8.1		-9.4		5.7	5.3
173	-2.1		-2.1		4.5	2.1
174	4.1		3.9		6.3	0.5
175	4.4		4.0		7.5	0.1
176	3.5	F	3.1	F	6.7	0.0
177	7.5	F	7.4	F	7.0	0.0
178	4.0		3.6		8.8	0.0
179	3.3	M	2.7	M	6.8	0.3
180	-23.6		-24.3		6.6	30.6
181	6.9		6.6		5.3	0.1
182	4.3		4.3		6.5	0.0
183	3.3		3.5		6.8	0.0
184	3.5		3.5		7.1	0.0
185	-22.3		-25.7		3.0	21.9
186	5.7		7.0		5.8	0.0
187	5.0		5.6		7.6	0.0
188	4.2		4.5		7.2	0.0
189	3.5	M	3.7	M	6.0	0.0
190	2.1	M	2.3	M	3.0	21.0
191	-18.1		-22.4		3.0	17.4
192	1.5		1.6		3.0	1.2
193	7.6		8.5		6.5	0.0
194	5.3		5.5		5.6	0.1
195	2.2		2.4		2.3	0.2

DOY	NE Lysimeter ET mm	Notes	SE Lysimeter ET mm	Notes	ETg mm	Precip mm
196	3.5	M	4.3	M	4.6	0.0
197	-1.3		-1.4		3.8	5.5
198	4.8	M	4.8	M	4.7	0.0
199	-10.9		-11.0		6.3	16.0
200	6.0		6.2		5.0	0.5
201	5.8		6.3		4.6	0.0
202	6.7		7.2		6.2	0.0
203	6.1	M	6.9	M	6.8	0.0
204	-6.3		-5.4		7.1	12.0
205	8.1		8.6		6.8	0.0
206	6.9		7.5		6.6	0.0
207	-11.8		-11.4		5.8	20.0
208	8.5		9.0		6.1	0.0
209	7.7		8.4		6.6	0.0
210	-6.6	M	-7.8	M	5.9	13.7
211	4.6		4.7		4.4	1.9
212	-5.1	M	-4.7	M	5.3	9.3
213	8.7		9.0		6.0	0.0
214	-10.6		-12.2		5.8	16.2
215	9.6		9.8		6.2	0.0
216	-6.6		-11.6		7.2	15.2
217	12.2		12.8		8.0	0.0
218	8.8		9.1		5.8	0.0
219	7.9	M	8.3	M	5.9	0.0
220	-20.3	M	-19.2	M	4.6	18.4
221	8.4		7.3		4.5	0.0
222	12.5		10.8		6.1	0.0
223	6.3		5.9		3.4	0.0
224	4.4		4.2		3.5	1.5
225	-13.4		-10.5		4.9	11.5
226	-35.6		-38.6		3.8	32.5
227	-2.1		-3.5		4.0	8.8
228	5.1		4.6		3.4	1.0

F=Equipment Failure
M=Maintenance